Advanced Composites and Hybrid Materials (2024) 7:125
https://doi.org/10.1007/s42114-024-00936-0

RESEARCH

Energy-safety balanced composites of attractive cyclic nitramines with polyaniline

Veerabhadragouda B. Patil[1] · Oldřich Machalický[2] · Petr Bělina[3] · Roman Svoboda[4] · Waldemar A. Trzcinski[5] · Svatopluk Zeman[1]

Received: 3 July 2023 / Revised: 10 May 2024 / Accepted: 3 July 2024 / Published online: 18 July 2024

Abstract
Composite microcrystals of the cyclic nitramines 2,4,6,8,10,12-hexanitro-2,4,6,8,10,12-hexaazaisowurtzitane (ε-CL-20), 1,3,5-trinitro-1,3,5-triazinane(RDX), 1,3,5,7-tetranitro-1,3,5,7-tetrazocane (β-HMX), and cis-1,3,4,6-tetranitrooctahydro-imidazo-[4,5-d]imidazole (BCHMX) with polyaniline (PANi) have been prepared and thoroughly characterized in terms of morphology and phase purity. PANi outperformed other conducting polymers in terms of selectivity towards NAs due to its better interaction with NAs, low production cost, and ease of preparation. The bonding of nitramines with the polymeric PANi chain has been examined by means of Fourier transform infrared (FTIR), Raman spectroscopy methods, and fluorescence quenching; the Raman spectrum has shown the laser sensitivity of these microcrystals. Powder X-ray diffraction results have shown changes in polymorph modifications in CL20 (from ε to β) and HMX (from β to α) during the preparation of the composites, which have also been confirmed by spectral and differential thermal analysis techniques. The structural orientations found in these composites significantly stabilize nitramines against impact; their detonation properties have slightly deteriorated, but the PANi electrical conductivity has strongly increased their electric-spark sensitivity. The above properties of the prepared composites determine their potential use mainly as parts of the electric or laser impulse initiators, having "a green character", for various charges.

Keywords Polyaniline · Nitramines · PANi-composites · Impact sensitivity · Electric-spark Sensitivity

1 Introduction

It is a well-known fact that the sensitivity of energetic materials usually increases with their performance [1, 2] (specifically with their energy content [3, 4]). Therefore, crystalline high-energy-content materials (HEMs), such as nitramines, need to be desensitized before being filled into the objects of their final use. For this purpose, it is suitable to use not only various methods of modifying the shape and grain size of these HEMs (for example [5, 6]), especially the coating of their crystals with suitable polymers (for the history and new trends, see [7]), which significantly increases the safety of handling during filling and application processes.

The electrically conductive polyaniline (PANi) [8] stands somewhat aside when it comes to the above-mentioned polymer applications. It has been tested successfully to reduce the risk of ignition caused by electrostatic-discharge (ESD) hazard in the processing and handling of 1,3,5,7-tetranitro-1,3,5,7-tetrazocane (HMX) and pentaerythritol tetranitrate (PETN) in the amount of 5 wt.% in a mechanical mixture

✉ Veerabhadragouda B. Patil
iamveerabhadraa@gmail.com

✉ Svatopluk Zeman
svatopluk.zeman@upce.cz

1 Institute of Energetic Materials, Faculty of Chemical Technology, University of Pardubice, CZ 532 10 Pardubice, Czech Republic

2 Institute of Organic Chemistry and Technology, Faculty of Chemical Technology, University of Pardubice, CZ 532 10 Pardubice, Czech Republic

3 Department of Inorganic Technology, Faculty of Chemical Technology, University of Pardubice, CZ 532 10 Pardubice, Czech Republic

4 Department of Physical Chemistry, Faculty of Chemical Technology, University of Pardubice, Studentská, CZ 532 10 Pardubice, Czech Republic

5 Faculty of Advanced Technology and Chemistry, Military University of Technology, 00 908 Warsaw, PL, Poland

(the authors have measured the specific volume resistance of these mixtures) [9]. Effective desensitization of nano-thermite to mechanical and electrical stimuli by the application of a coating of 1–5 wt.% of PANi to nanoparticles of this energetic mixture [10].

Polyaniline was chosen because of its permanent conductivity and stability and, above all, because of its economic and technical availability. Other conductive polymers do not match the availability and stability of PANi. Other conducting polymers, like polyfuran, polypyrrole, and polyphenylene vinylene, are relatively stable under certain conditions but can degrade over time and, at the same time, are not cost-effective [11]. Researchers have evaluated graphene oxide, which is also used as an additive in composite formulations, only in terms of its influence on the sensitivity to impact and friction [12–14], not to electrical spark. This oxide might be as effective as PANi, which outperforms this oxide by better interaction with NAs and the aforementioned ease of preparation and cost advantage.

As shown by recent studies, PANi also has fluorescence properties [8, 15–18] (it acts as a fluorophore—see the "fluorescence study" section). It also forms charge-transfer complexes with polynitro compounds, in which it acts as a fluorescent sensor, with application in the quick trace spectrochemical detection of explosives [15–18]. The structure of the mentioned complexes of nitramines with PANi (see Scheme 1) [15, 16] indicates that they might have a beneficial effect on the reduction of the initiation reactivity of these polynitro compounds. Therefore, this possibility is investigated in this paper, taking into account the most attractive cyclic nitramines 1,3,5-trinitro-1,3,5-triazinane (RDX), ß-1,3,5,7-tetranitro-1,3,5,7-tetrazocane (ß-HMX), ε-2,4,6,8,10,12-hexanitro-2,4,6,8,10,12-hexaazaisowurtzitane (ε-CL-20), and cis-1,3,4,6-tetranitrooctahydroimidazo-[4,5-d]imidazole (BCHMX or bicyclo-HMX).

The study also focuses on the verification of the feasibility of the co-agglomeration method (sludge cocrystallization method) [6, 19–22] for the preparation of mixed crystals (composites) of attractive nitramines with non-explosive PANi-polymer. Using spectroscopic methods (Raman, FTIR, and, newly, fluorescence), attention is focused on the specific relationships between the molecular structure and the initiation reactivity of these composites; most of these relationships have novelty and are potentially helpful for computational chemists too. In relation to this reactivity, the study of the explosive and stability properties of nitramine/PANi complexes is also the main subject of this research, with an estimation of the possibility of their practical use as explosive fillings for various military and civilian objects. Especially the latter area could be prospectively related to the development of "green primers" for electric detonators and airbag initiators, i.e., replacement of environmentally undesirable lead salts of 2,4,6-trinitroresorcinol, picraminic acid (2-amino-4,6-dinitrophenol), and azoimide, used in them so far.

2 Materials and methods

2.1 Nitramines (NAs) and polyaniline (PANi)

ε-2,4,6,8,10,12-Hexanitro-2,4,6,8,10,12-hexaazaisowurtzitane (ε-CL-20) was procured from the Explosia Co. pilot plant in Pardubice; it was purified by ethyl acetate/n-heptane employing the solvent/antisolvent crystallization method. 1,3,5-trinitro-1,3,5-triazinane (RDX) was a product of the former Chemko Co. in Strážske (Slovakia), whereas cis-1,3,4,6-tetranitrooctahydroimidazo-[4,5-d] imidazole (BCHMX or bicyclo-HMX) was prepared at the Institute of Energetic Materials (IEM) according to a protected method [23]. α-1,3,5,7-tetranitro-1,3,5,7-tetrazocane (α-HMX) was obtained by precipitation of a larger volume of the β-HMX solution in dimethyl sulfoxide–methanol (1:1) by a water–methanol mixture (1:1). Technical polyaniline was prepared at the IEM [15, 16]. Nitramines (NAs) were desensitized by introducing 16–20 wt.% of PANi.

2.2 The preparation of co-agglomerated composites (CACs)

Polyaniline composite crystals with attractive nitramines (NAs/PANi) were mainly produced by a two-step procedure (i.e., by co-precipitation followed by an attempt to co-agglomerate these co-precipitates [19]), in which 4 g of the respective nitramine (separately HMX, BCHMX, CL20 or RDX) were dissolved together with 1 g of PANi in DMSO. After a clear solution was obtained, it was co-precipitated by pouring into vigorously stirred water. The co-precipitates obtained were filtered and dried and then placed into 30 ml of chloroform (continuous phase), and the resulting suspension was allowed to boil gently with continuous stirring for 4 h. The NAs/PANi obtained were filtered and dried. They were coded as 57 CL20/PANi, 58 HMX/PANi, 59 BCHMX/PANi and 60 RDX/PANi. Furthermore, these CACs were characterized thoroughly in terms of morphology and phase purity.

3 Experimental part

3.1 Powder X-ray diffraction (PXRD) studies

The peak intensities at 2Θ values have been obtained using the PXRD technique. They are summarized in Table 1 and documented by the PXRD diffractograms in Fig. 1 (for all diffractogram peaks, see Fig. S3 and Table S1 in

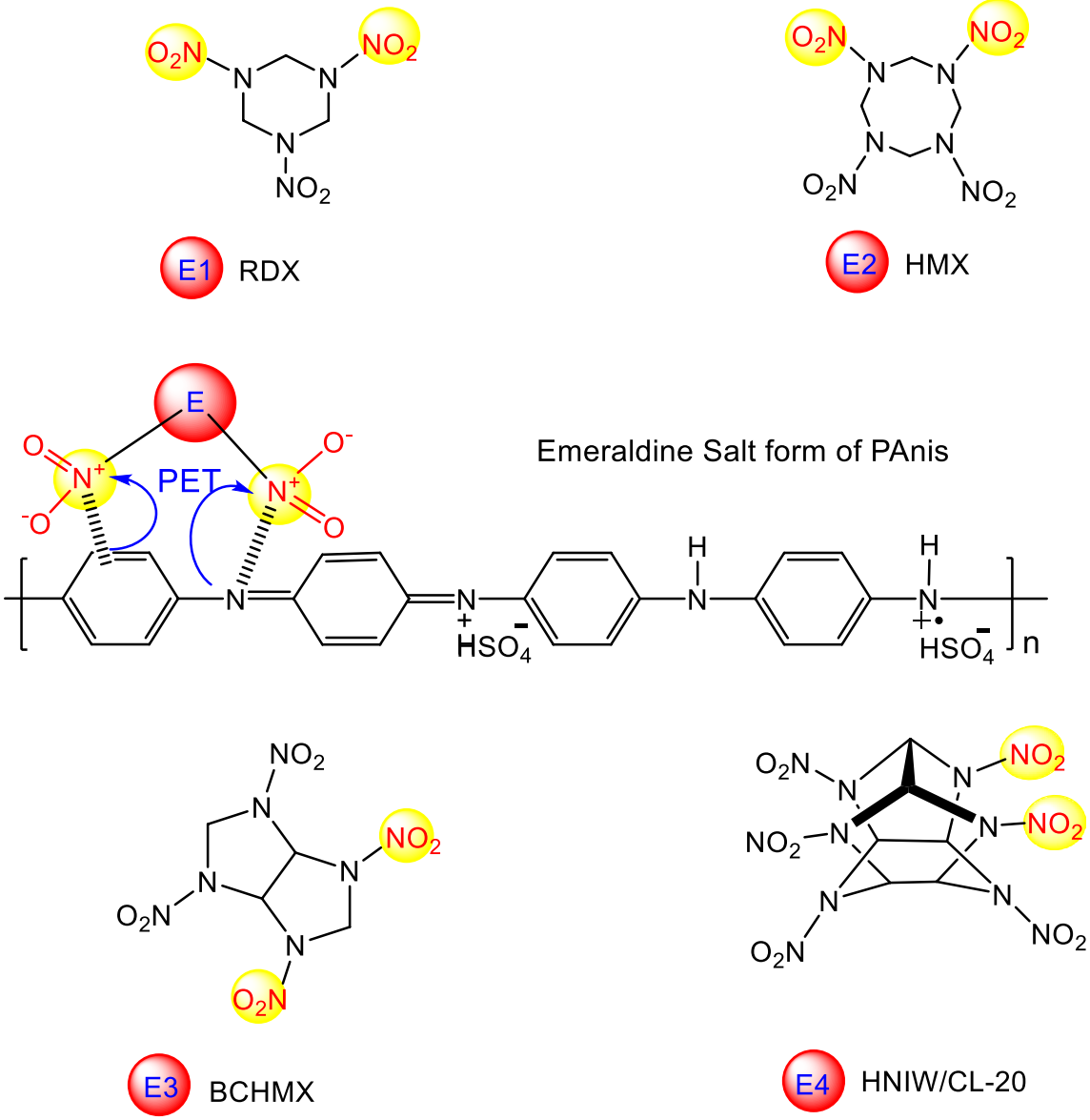

Scheme 1 A schematic representation of polyaniline composite crystals; the binding of attractive nitramines with the PANi chain to form complexes with the charge transfer (for the sake of continuity in works codenamed CACs) between the NA and PANi molecules of the contact surfaces of these two co-formers—recreated from a previously reported work [15]

Supplementary Information). The nitramines (NAs) with PANi undergo co-agglomeration—binding to the PANi polymer chain (Scheme 1). The changes associated with it are clearly observable in PXRD diffractograms. The NAs act there as Lewis acids with electron-withdrawing groups, easily binding electrons from the PANi chain (Scheme 1). This stabilizes the polymeric PANi-NA chain. The achievement of this compactness in the polymeric chain is accompanied by the following polymorphic changes of some nitramines: ε-CL20 is converted into its β-modification with the formation of the β-CL20/PANi composite, whereas β-HMX is transformed in its polymorphic α-modification, in which it is stabilized in the corresponding α-HMX/PANi composite crystals. In earlier papers, HMX was stabilized in its co-agglomerated crystals (CACs) with polynitro arenes [19, 20] and polynitramines [6] in the form of their δ-modification. In co-crystals with polynitro compounds, CL20 is present mostly in its β-polymorph [24]. On the other hand, in co-crystals with non-nitrate compounds, it enters into the co-crystal lattice in its γ-modification. In this sense, PANi seems to be an exception—as the nitro group free polymer (with a very low nitrogen content), has initiated the formation of β-CL20 not only in the polymeric PANi-NA chain (see more details in the "Discussion" section).

Table 1 PXRD data for pure nitramines and CACs

Sr no	Code design	2Θ values for intense peaks (%)
1	ε-CL-20	14.30, 30.10, 42.98
2	β-CL-20	12.66, 13.86, 30.34
3	BCHMX	9.74, 12.65, 23.57
4	β-HMX	14.61, 16.31, 24.45, 25.07, 32.31
5	δ-HMX	13.10, 17.02, 24.34
6	RDX	9.73, 12.65, 23.59
7	PANI	20.50, 25.44
7	57 CL20/PANi	11.98, 13.66, 20.06, 27.88
8	58 HMX/PANi	20.52, 27.20, 29.66, 31.94
9	59 BCHMX/PANi	9.98, 12.92, 16.18, 23.84
10	60 RDX/PANi	13.00, 17.28, 20.30, 29.22

Complete diffractograms of minor peaks at 2Θ values of the CACs are shown in Supplementary Information Table S1

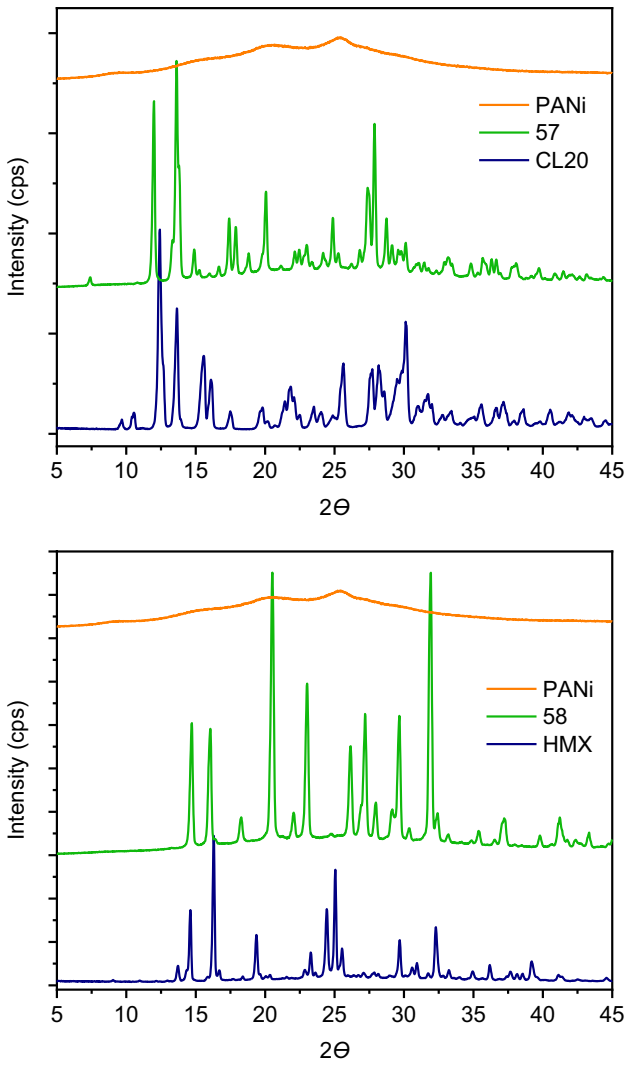

Fig. 1 PXRD diffractograms of the composites (CACs) 57 CL20/PANi, 58HMX/PANi, 59 BCHMX/PANi and 60 RDX/PANi

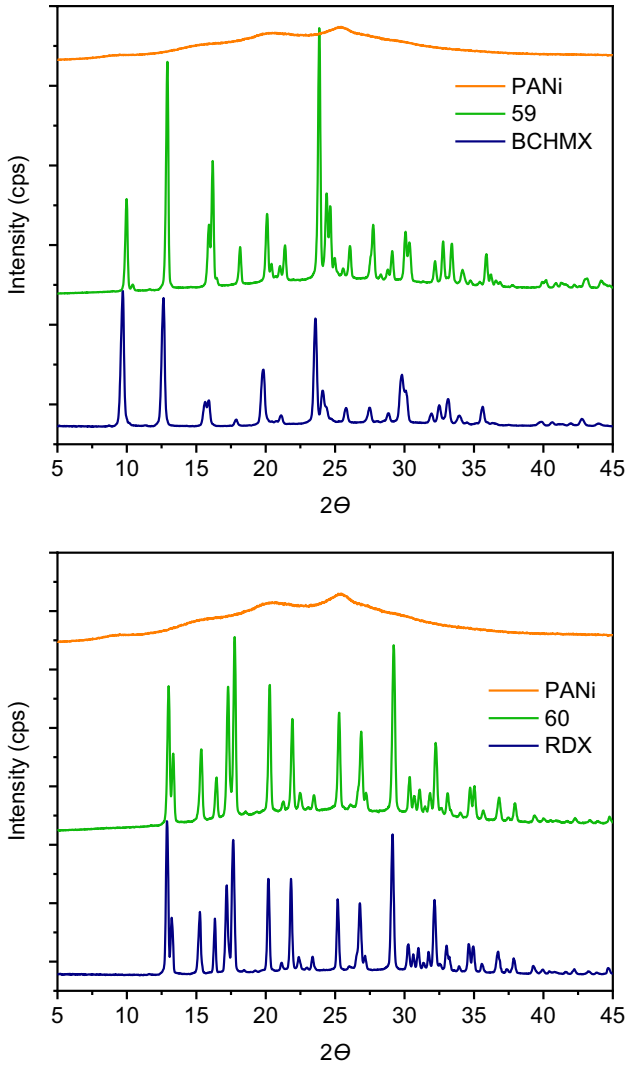

Fig. 1 (continued)

These changes in modifications are evaluated below using DTA, where endothermic changes are matched with PXRD data. Nitramines have been shown to form complexes with PANi with polycrystalline microparticles in a different way than in classic co-crystal formation (in terms of intermolecular interactions); therefore, they may be referred to as PANi doped with NAs. More broadly, labeled them here as NA-PANi composites. As shown in morphology and FTIR examinations and illustrated by Scheme 2, two major kinds of these composite crystals are formed.

3.2 Morphology and particle-size analysis

The morphological changes in nitramine crystals after binding with the polymeric chain of PANi were analyzed employing FESEM analysis. The FESEM results obtained are reported in Fig. 2a–h (for pure PANi SEM images, see Supplementary Information Fig. S1). The structures of the

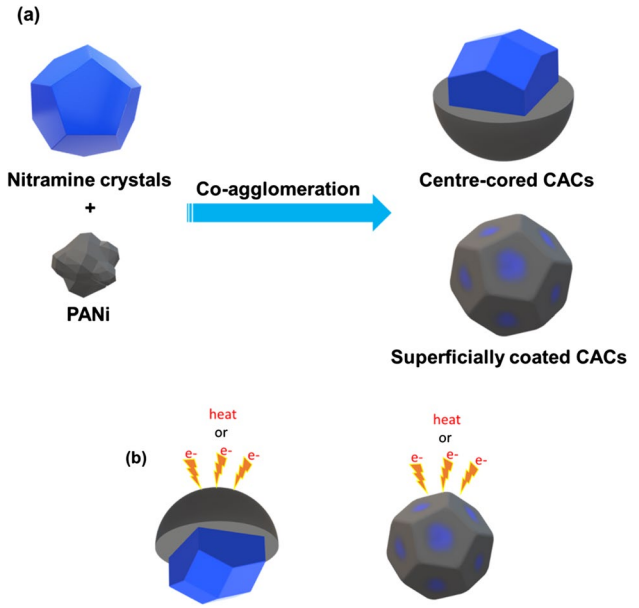

Scheme 2 A schematic representation of two kinds of CACs. **a** The nitramine center-core crystals surrounded by PANi and superficially coated with PANi, the latter of which have made the edges of nitramine CACs smoother (rounded); **b** both of these partial schemes with the indicated action of heat (during DTA measurements) and electron (during electric-spark sensitivity measurements) transfer to the composites

CACs of CL20 and BCMHX resembled smoother spherical peanuts, whereas the CACs of HMX and BCHMX appeared in the form of different smoother-surface irregular sticks resembling crystals. The smoother surface is common in all NAs/PANi; it shows that the crystals have been coated with PANi, which has smoothed the crystal edges. This indicates the possible formation of core-centered complexes with PANi. These smoother surfaces can be effectively influenced in impact sensitivity tests; they have made nitramines in CACs withstand higher drop energy (see Table 8). Overall, this shows that PANi has acted as an effective phlegmatizer for selected attractive nitramines (the effects of phlegmatization are shown in Scheme 2). Also because of this core-centered crystal effect, the densities of CACs are maintained (see Table 7).

In addition to morphology, it is very important to analyze particle size and NA/PANi-specific surface areas (see section S2.7 in the Supplementary Information for details on the instruments). As can be seen from Table 1, the co-agglomeration of NA/PANi co-precipitates in chloroform leads to the largest increase in specific particle surface area for RDX/PANi and β-HMX/PANi composites. RDX nanoparticles are known to have the greatest propensity to self-agglomeration [25]. This agglomeration is relatively small for β-CL20 and α-HMX analogs; for BCHMX/PANi, it is rather milling than agglomeration. Together with the surface morphology, these parameters also help NAs/PANi resist higher droplet energy (see the sensitivity discussion for more details).

3.3 Differential thermal analysis (DTA)

The thermal stability of the composites prepared was evaluated employing the DTA 550 Ex apparatus (like in papers [6, 19]—OZM Research, Czech Republic; for instrumental details, see section S2.5 in the Supplementary Information.). The thermograms obtained are shown in Fig. 3, and the results are summarized in Table 2. PANi decomposes at 600 °C, which is not important here; the main focus is on the thermal stability of its composites. Figure 3 shows

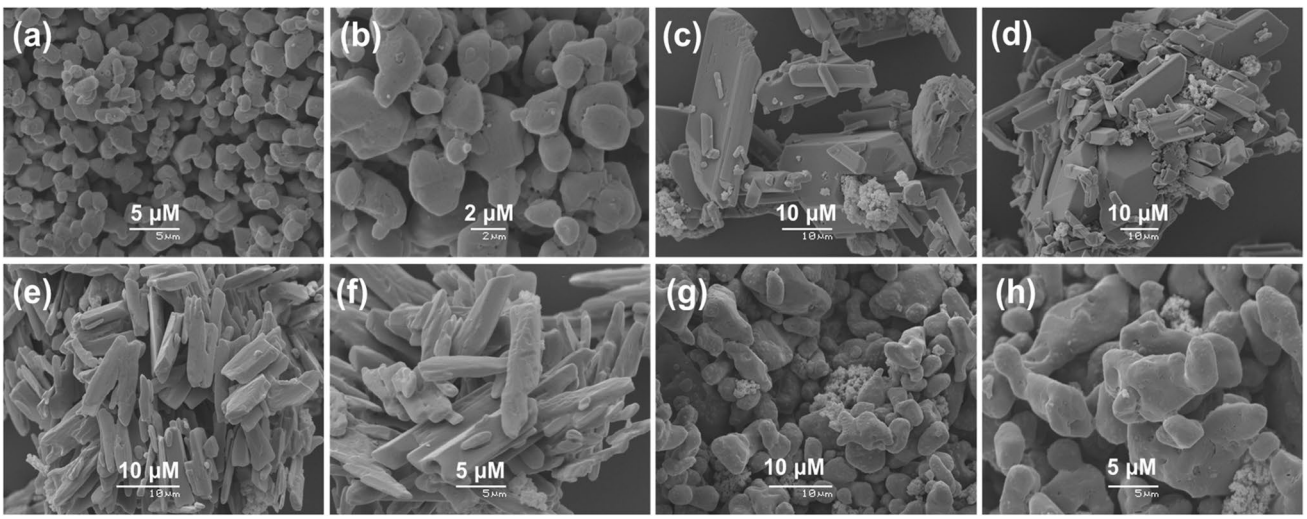

Fig. 2 FESEM images of the composites **a** and **b**, 57CL20/PANi; **c** and **d**, 58 HMX/PANi; **e** and **f**, 59 BCHMX/PANi; and **g** and **h**, 60 RDX/PANi

Table 2 Particle-size measurements

Sr no	Code design	Surface area (m^2/kg)	Dv(10) µM	Dv(50) µM	Dv(90) µM
1	57p CL20/PANi	1740.00	1.59	6.89	25.60
2	57 CL20/PANi	1764.00	1.76	6.79	40.50
3	58p HMX/PANi	724.50	4.11	18.21	51.20
4	58 HMX/PANi	788.61	3.89	18.70	80.60
5	59p BCHMX/PANi	1318.00	1.94	7.68	28.10
6	59 BCHMX/PANi	1233.01	2.06	8.35	40.10
7	60p RDX/PANi	774.50	4.07	15.60	83.80
8	60 RDX/PANi	1126.01	2.80	9.66	40.40

The samples with "p" are those obtained from the first step of co-agglomeration, i.e., co-precipitates

that the onsets of the CAC thermal decomposition are in all cases lower than those of pure NAs. Logically, the peak temperatures of their exothermic decomposition are slightly decreased as well (see Table 3). The decrease in the thermal stability of the composites in comparison with pure nitramines may be caused by the mechanism of their interaction with the building units of the PANi chain, as shown in Scheme 1. The indicated mode of interaction should facilitate the homolysis of the N−N bond. In addition, the chain contains hydrogen-sulfate, i.e., acidic, anions. The intensity of the interaction in the composite is so high that exothermic decomposition appears in the original thermal range of the CL20 polymorphic transition. Similarly, in a composite with HMX, the decomposition also starts in the region of its α–δ transition. It is evident from Fig. 3 that RDX, bonded on the PANi chain, begins to decompose in a solid state of this complex, which is a big difference from the thermolysis of its CACs with polynitro compounds [6, 19, 20].

3.4 FTIR spectral studies

For the confirmation of the intermolecular interactions between PANi and nitramines, spectral studies were employed, with FTIR showing some interesting results. The Nicolet Protege 460 FTIR spectrometer was utilized to record the IR spectral measurements of the samples using the transmission technique. The spectra obtained are shown in Fig. S5 in the Supplementary Information, and characteristic peak shifts at the wavelengths are summarized in Table 4. These spectra are sufficient for the identification of peak shifts with clear separations. The spectra have shown absorption peaks in the wavelength region, i.e., 1480 ± 20 and 1565 ± 20 cm^{-1}, which are characteristic of the stretching vibrations of C=C quinoid and benzenoid rings, respectively. Similarly, the peak lengths of polarons and quinoids indicate the presence of polaron and bipolaron in different ratios in the polymer chain [26] (based on the peak lengths,

Table 3 Summarized data from DTA thermograms of co-formers and CACs with visible melting points

Samples	Melting point (°C) [ref.]	Peaks of changes in DTA record, °C (change of modification)	
		Endothermic	Exothermic
ε-CL-20	240 decompn [20]	170.01 (ε–γ)	225.01 (γ–δ)
α-CL-20[a]	240 decompn [20]	175.00 (α–γ)	225.01 (γ–δ)
BCHMX	286 decompn [20]		224.00
α-HMX		189.60 (α–δ)	272.00
RDX		209.01	215.01
PANi		NA	155.78, 243.25, 246.90, 251.36
57 CL20/PANi		NA	218.92
58 HMX/PANi		179.40 (β–δ)	265.95
59 BCHMX/PANi		NA	218.53
60 RDX/PANi		NA	199.19, 217.56

[a]In this hemihydrate between 90 and 105 °C, there is a very weak, elongated endotherm of crystal-water evaporation

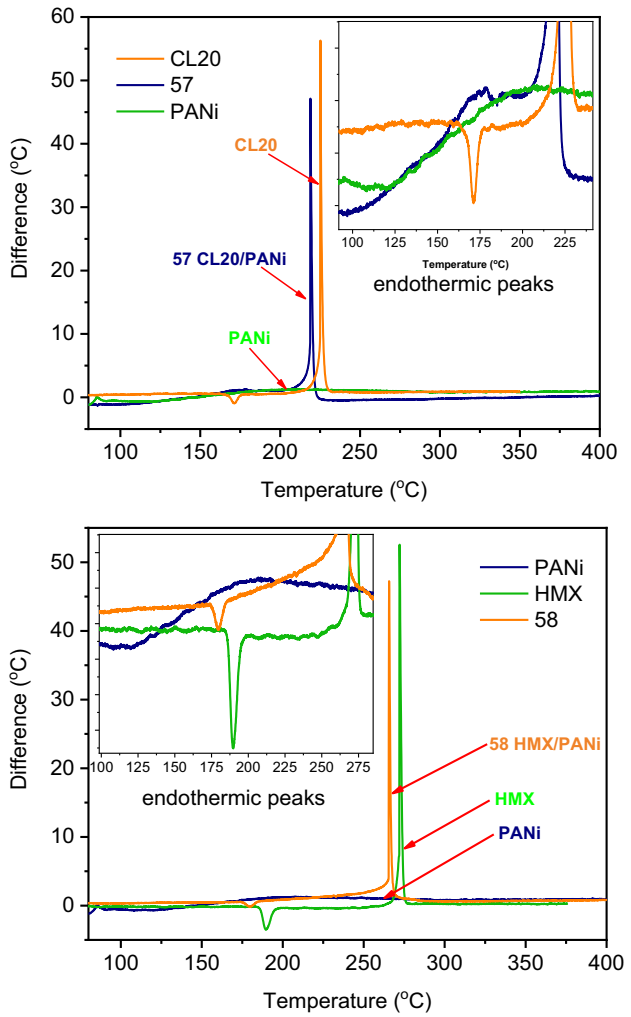

Fig. 3 DTA thermograms of the composite crystals 57 CL20/PANi, 58 HMX/PANi, 59 BCHMX/PANi, and 60 RDX/PANi

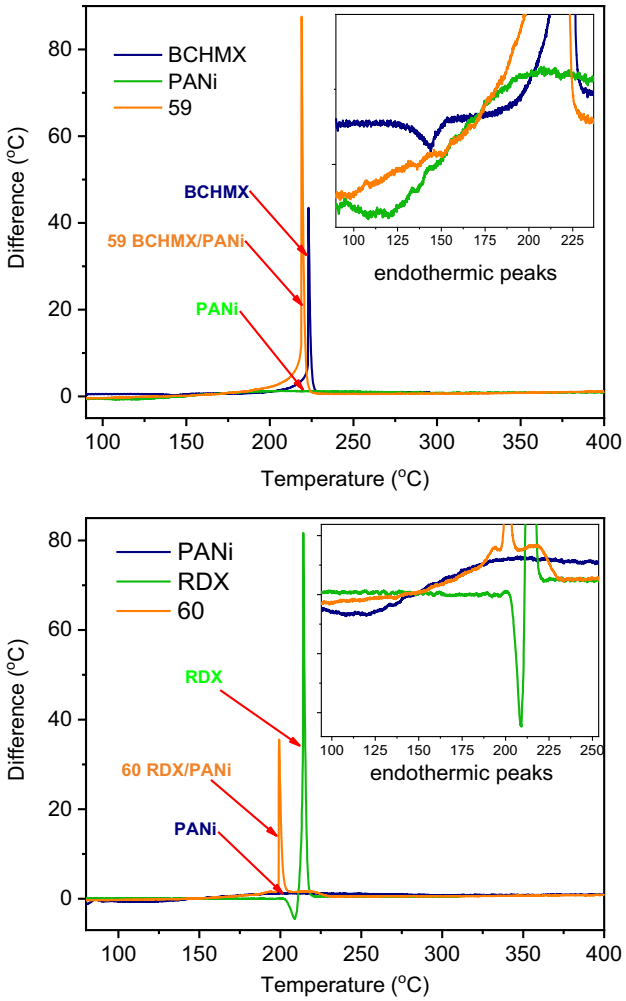

Fig. 3 (continued)

it is possible to determine the ratios of polarons and bipolarons). If this ratio is equal to one, there is an equilibrium between them; if not, there is no equilibrium. In this study, there is no equilibrium between them. This means that there is a form of the emeraldine salt of PANi [15] that will further strongly influence the sensitivity to the electric spark (see the discussion of the energy aspect).

Having undergone co-agglomeration, individual nitramines show different blue shifts; in CL20, due to its molecular crowdedness (slight repulsion with rings of the PANi chain), there might be only its partial interaction with PANi and thus some surplus amount of free β-CL20 in the mixture. On the other hand, electrostatic attraction with short contacts in the other nitramines causes bond elongation within the polymeric chain, resulting in a red shift. These observations clearly indicate that the addition of nitramines will be followed by a rapid transition process in both rings (benzenoid and quinoid in PANi). This further affects the formation of the NA-PANi complex with an electron-transfer mechanism (Scheme 1). Moreover, there are significant changes in the C–N stretching of both primary and secondary aromatic amine groups as well as in bipolaronic B–$NH^{+\bullet}$–B peaks. In addition, the nitramines exhibit significant $-NO_2$ stretching vibrations. From DTA and PXRD data, it is commonly known that CL20 changes its polymorphic form ε to β-form, which sits in the polymeric chain more conveniently. However, β-CL20/PANi might exhibit a low amount of the unbound pure nitramine also in this composite. Except for this, RDX and BCHMX have shown good compatibility with PANi. The peak observed at 675 ± 20 cm^{-1} corresponds to the bending vibration of the HSO_4^- group [27], which has been further confirmed by the Raman spectrum.

3.5 Raman spectral studies

Raman spectra were measured by a Thermo Scientific™ DXR3 Raman Microscope, employing an excitation laser

Table 4 Summarized results of FTIR measurements

Assignments	PANi	57 CL20/PANi	58 HMX/PANi	59 BC/PANi	60 RDX/PANi
N = Q = N quinonoid (Q) unit stretching	1563	1594	1525	1552	1568
N–B–N benzenoid (B) unit stretching	1480	1490	1459	1471	1458
(C–N) stretching of secondary aromatic amine	1290	1250	1259	1270	1262
(C–N) stretching of primary aromatic amine	1237	1227	1236	1207	1231
Q = NH + –B or B–NH + •–B	1032	1093	1085	1084	1037
Gamma (C–H) (1,4-disubstituted unit)/Q unit deformation	879	874	871	860	880
HSO_4; $-SO_4^{2-}$	696	687	657	654	671
Symmetric $-NO_2$ stretching	NA	1250	1259	1270	1262
Asymmetric $-NO_2$ stretching	NA	1553	1525	1529	1529
C–N stretching [amino group]	NA	762	771	774	752
C–N stretching [nitro group]	NA	1325	1324	1355	1349
Skeletal stretching [ring]	NA	1163, 1093	1137, 1085	1135, 1084	1131, 1037
N–O symmetric stretching	NA	1251	1260	1272	1261

source (the wavelength of 785 nm and the power of 29 mV), a × 10/0.25 objective, and the grating of 400 lines/mm (3378 to 49 cm^{-1}). The measured spectra are attached in Supplementary Information Fig. S4, and characteristic peak shifts are summarized in Table 2. However, the pure PANi and its composites are highly sensitive to laser power above 29 mV with × 10/0.25 grating (for more instrumental specifications, see the Supplementary Information section S2.8). If this laser power is exceeded, the Raman spectrum shows mainly two peaks, namely polaronic charge carriers (−C–N•+) and the −C = C stretching vibration of the semiquinoid ring [15, 18]. Unlike in FTIR, the Raman spectrum shows polaron interaction [15]. The current study focuses on the measured interactions between the nitramines and the PANi chain. Therefore, we have taken lower spectral laser peaks with optimal peak separation. The appearance of the small peak at 185 ± 10 indicates the presence of PANi in emeraldine salt form II as well as the presence of the HSO_4^-anion [27]. In both FTIR and Raman spectroscopy, this implies sulfuric content in pure PANi as well as CACs, which is further confirmed by elemental analysis (see Table 7 and supplementary information Table S2). Like in FTIR, benzenoid and quinoid peaks show significant variations, which can be seen from the characteristic peak shifts summarized in Table 5.

3.6 Fluorescence studies

Fluorescence measurements were carried out using a PTI Quantamaster 30 fluorometer (Horiba Scientific) as an additional instrument to determine the influence of the charge-transfer complex formation in the CACs (NAs/PANi—see Scheme 1) on their properties. The outputs of these measurements in the DMSO solution are presented in Fig. 4, where the first absorption band at ca 630 nm is probably a mixture of n–π* and π–π* transitions and the short wavelength absorption band on the UV–Vis spectrum at ca 330 nm corresponds to the π–π* transition of the PANi macromolecule [15–21, 26–29]. The maximum on the fluorescence excitation spectrum for PANi is shifted bathochromically about 25 nm away from the short-wavelength absorption band. The PANi used is a mixed oxidation-state polymer compound of reduced benzenoid units and oxidation quinoid units; the very weak fluorescence emission does not come from the actual PANi macromolecule, but it is caused by the presence of fewer PANi chains with reduced benzenoid units in this polymer [8] (see the Supplementary Information S2.12 section for details). However, the weak fluorescence emission allowed us to determine the quantum yields more or less extrapolatively in very small values. Therefore, the same was used for relative fluorescence quantum yields (RFQY) with respect to the RDX/PANi yield (which had this value the highest). Nevertheless, the application of these RFQYs in the study of the properties of NA/PANi composites has yielded logical and interesting results, as shown below.

Figure 4 clearly demonstrates that the NA-PANi complex formation leads to a decrease in fluorescence, i.e., to fluorescence quenching [15–18]. Nevertheless, there will still be a small amount of a free moiety of PANi. Electrons in the polymer chain will be delocalized and the NA-PANi

Table 5 Summarized results of Raman measurements

Assignments	PANi	57 CL20/PANi	58 HMX/PANi	59 BC/PANi	60 RDX/PANi
Phenazine-like crosslinking	1703	1619	1620	1620	1669
C ~ C stretching vibrations of the semi-quinoid unit	1592	1593	1598	1601	1591
N–H deformation in the semi-quinoid structures	1506	1504	1510	1509	1502
C ~ N + • stretching vibrations in highly localized polarons	1376	1378	1376	1379	1380
C ~ N + • stretching vibrations of the semi-quinone cation radicals in delocalized polaronic structures	1339	1332	1349	1339	1334
C–N stretching in benzenoid and quinonoid structures	1232	1267	1267	1267	1269
C–H deformation vibration of a quinonoid unit	1169	1170	1172	1174	1169
The benzene-unit deformation in the emeraldine salt	809	805	881	850	846
Phenazine-like crosslinking	575	579	597	578	575
Out-of-plane unit deformations in the emeraldine base	413	414	413	416	414
Asymmetric $-NO_2$ stretching vibration	NA	1570, 1593	1578, 1598	1567, 1597	1560, 1591
Symmetric $-NO_2$ stretching vibration	NA	1285, 1267	1267, 1248	1267, 1259	1269, 1250
$-NO_2$ deformation vibration	NA	841, 805	844, 806	848, 803	882, 805
$-NO_2$ wagging	NA	737, 718	735, 719	735, 715	732, 715
−N−N bond stretching	NA	1169	1170	1172	1171

linkage will provide easy access to external electric charges. These are the main reasons for the electric-spark sensitivity of CACs (see Table 8 and the discussion of sensitivity in Fig. 10). Further structural changes have been confirmed by relative fluorescence yield analysis (Figs. 4, 6b, 7c, 8a and b, and 9a).

Similar behavior has also been found in the case of samples 57, 58, 59, and 60. The RFQYs related to the absorption band at ca 330 nm are summarized in Table 6. Quantum yield, in general, is known to decrease if a non-fluorescent molecule is bound to a fluorescent molecule. The binding between the NAs and PANi decreases the quantum yield, which can be explained by the Lippart equation [28]. The non-fluorescent compound (NA) bound to a fluorescent material (PANi) changes the quantum yield; consequently, the excited delocalized electrons are absorbed by NAs (via the NA-PANi linkage), which causes non-radiative decay (K_{nr}) in the complex [28].

3.7 Thermochemical and explosive properties

The heat of combustion of pure nitramines and their PANi-composites (more details are available in the Supplementary Information section S2.10) was considered for the calculation of thermochemical parameters. Density was measured experimentally using a densitometer, and the composition of the composites was obtained from elemental analysis (see section S2.9 in the Supplementary Information). The enthalpy of formation was calculated using these data and Hess's law. The results obtained are summarized in Table 7 and graphically represented in Fig. 10.

The density of PANi is relatively low compared to the nitramines; after PANi treatment by NAs, the composites produced have an interesting arrangement (Scheme 3), with crystals of relatively similar or in some cases slightly higher density than pure nitramines (it is caused by the polymorph transition of ε to β in CL20 and β to α in HMX).

All of these data were utilized for detonation-property calculations using the CHEETA code [30] (see section S2.3 in the Supplementary Information). Some of the mechanical and thermal energy was collectively considered detonation energy here. The volume of detonation products considered up to a pressure of 1 atm determined the mechanical energy, which is equal to the expansion work of the detonation products, and the thermal energy, which is the heat in the detonation products under this pressure [31–33]. Other conditions, a temperature of 1800 K on the isentrope beginning at the CJ point, and the composition of detonation products under these temperature conditions were considered for the calculations.

Another important issue is the impact and electric-spark sensitivity of the CACs studied; impact sensitivity was determined by means of a standard impact tester (Julius Peters [34] as shown in Fig. S2a in Supplementary Information) with an exchangeable anvil, with the amount of the tested substance being 50 mm^3 and the drop hammer used weighing 2 kg, as described in previous paper [6]. This sensitivity is expressed in the following mainly in terms of the hammer fall energy (also drop energy, E_{dr}, in J) for a 50% probability of initiation (detected by ear as an explosion), but additionally, this energy can be reported also for a 95% probability of initiation (both

Table 6 Relative fluorescence quantum yields of the samples under study measured in DMSO

Sample	Relative quantum yield
PANi	0.57
57 CL20/PANi	0.50
58 HMX/PANi	0.86
59 BCHMX/PANi	0.97
60 RDX/PANi	1.00

Table 7 The molecular formulas, thermochemical properties, and the maximum crystal density of pure substances and the corresponding CACs

Explosive					Heat of combustion[a]		Enthalpy of formation		Crystal density ($g.cm^{-3}$)
No	Code design	NAs/PANi[c]	Formula[b]	Mol. weight	Q_c ($J.g^{-1}$)	Ref	ΔH_f (kJ. mol^{-1})	Ref	
1	RDX		$C_3H_6N_6O_6$	222.14	9522	[36]	66.2	[36]	1.810
2	BCHMX		$C_4H_6N_8O_8$	294.17	9124	[36]	236.5	[36]	1.860
3	α-HMX		$C_4H_8N_8O_8$	296.18			75.02	[37]	1.839
4	β-HMX		$C_4H_8N_8O_8$	296.18	9485	[36]	77.3	[36]	1.902
5	ε-CL20		$C_6H_6N_{12}O_{12}$	438,23	8311	[36]	397.80	[36]	2.044
6	β-CL20		$C_6H_6N_{12}O_{12}$	438.23	8327	[37]	421.74	[37]	1.985
7	PANi		$([C_6H_4NH]_2[C_6H_4N]_2)_n$	95,800 [29]	24,497	[Cw]	158.57	[Cw]	1.5022
			$C_{6.00}H_{6.33}N_{0.98}O_{2.00}S_{0.14}$	128.64					
8	57 CL20/PANi	1.0:0.2	$C_{10.66}H_{11.01}N_{12.00}O_{14.62}S_{0.17}$	546.59	11,240	[Cw]	321.47	[Cw]	1.9691
9	58 HMX/PANi	1.0:0.2	$C_{6.66}H_{10.16}N_{8.00}O_{9.02}S_{0.13}$	354.58	11,979	[Cw]	31.19	[Cw]	1.8967
10	59 BCHMX/PANi	1.0:0.2	$C_{6.35}H_{8.00}N_{8.00}O_{8.82}S_{0.05}$	333.40	11,245	[Cw]	89.21	[Cw]	1.8916
11	60 RDX/PANIi	1.0:0.2	$C_{5.09}H_{8.60}N_{6.00}O_{6.71}S_{0.08}$	263.72	12,379	[Cw]	6.17	[Cw]	1.8295

Cw refers to results obtained in the current work

[a]The values of the heat of combustion are shown in Table S3 in the Supplementary Information

[b]Hypothetical formulas of the CACs and PANi have been calculated from the elemental-analysis results shown in section S2.9 of the Supplementary Information

[c]NAs/PANi means the molar ratio of the nitramine/PANi

these variants see Table 8). Electric-spark sensitivity [35] was determined as an energy of an electric spark for a 50% probability of initiation (E_{ES} in mJ) using a device with electrodes in direct contact with the sample (the ESZ 2000 MIL apparatus of the company OZM Research, Fig. S2b in Supplementary Information). The results of both of these mentioned test methods are summarized in Table 8, and their methodological details are available in the Supplementary Information section S2.4. It is interesting and important that because of morphological changes (Figs. 4 and 7a, Scheme 2) in CACs, the presence of PANi improves their resistance to impact; on the other hand, due to the conductivity of PANi, these NA/PANi composites show higher electrical sensitivity. PANi thus acts as a passage for the transfer of electrons to the reaction centers of nitramine molecules (their addition to nitro groups [35]), which makes composites more sensitive to an electric spark than their pure forms.

4 Results and discussion

4.1 Co-agglomeration

The attempt at co-agglomeration was preceded by the preparation of mixed microparticles by co-precipitation from a common solution. The particle size and surface area of the NA/PANi composites in both of these processes were actively

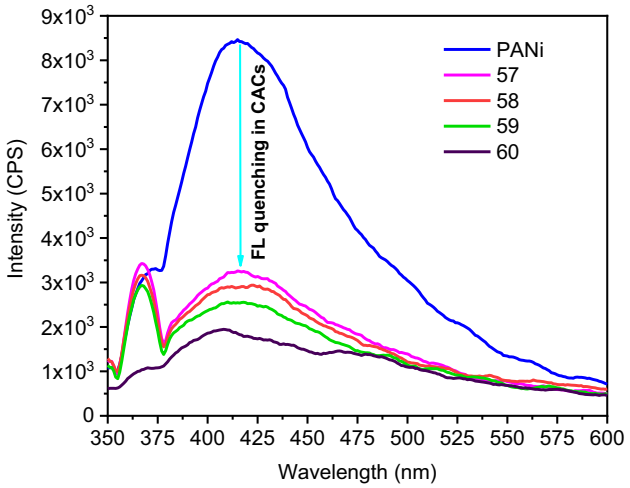

Fig. 4 The fluorescence spectrum of pure PANI and its NA-composites in DMSO

influenced by intense stirring (see Table 2). However, real, mild co-agglomeration was observed only in the case of BCHMX/PANi; in the other mixed co-precipitates, there was an increase in the specific surface area after the co-agglomeration operation. This was further confirmed by the analysis of the particle sizes of the co-precipitates and the final composites (see Table 2). Therefore, referred to as "co-agglomeration" here, as an applied process (to maintain continuity with previous publications [6, 19, 20]), it results in composite microparticles. The results obtained are summarized in Table 2. The co-agglomeration process has also shown improvement in the surface morphology of the CACs—as observed from the FESEM analysis, the crystals had smoothed surfaces in all the cases. FESEM images showed two major kinds of crystals, namely center-core and coated, which made the edges of nitramine crystals smoother (rounder) (see Scheme 2). As an exceptional case, the β-CL20/PANi center-core crystals have unequally distributed average crystals.

4.2 Thermal analysis

As earlier mentioned, the interaction of the nitramine molecules with the building units of the polyaniline chain in the sense of Scheme 1 leads to their thermal destabilization. This could be explained as follows: This interaction of the π-electron system or the free electron pair of aniline nitrogen (complexes with charge transfer) with the nitro group counteracts the mesomeric effect (Scheme 3) in the nitramine grouping by reducing the charge deficiency on the nitrogen atom of the nitro group (the balance is then shifted to the left side and the N−N bond should thus be weakened).

The morphological changes connected with the formation of the complexes with charge transfer have effectively influenced the thermal analysis of the composites prepared (Table 2 and Fig. 3). Considering the structure of these complexes (Schemes 1 and 2) and the corresponding morphological changes (Fig. 2 and Table 2), the heat transfer will first take place through the PANi chain with subsequent transfer to the nitramine molecule.

4.3 Spectral examination

In spectral observations, the stretching, bending vibrations, and vibrational modes of PANi are predominant because the composites of the NA crystals are shielded by PANi (Scheme 2). From the spectral characterizations, it is known that nitramines are bonded with the polymeric chain with the electro-force of attraction with the formation of short contacts with the benzenoid ring, quinoid units, and polarons. These bonds are formed during the "co-agglomeration" of the applied heat, which helps the electron-enriched PANi attach with the electron-deficient nitro groups of nitramines. Except for the β-CL20/PANi complex, the composites have several possibilities of complex formation (see Scheme 2). Additionally, PANi and all of its composites prepared have been found laser-sensitive; therefore, to avoid their ignition during analysis, the minimum laser power (29 mV with × 10/0.25 grating) has been used.

FTIR and Raman stretching vibrations overlap with each other and thus verify that there is a complex with charge-transfer formation in PANi CACs. The electron transfer during "co-agglomeration" leads to complex formation, which is explained using molecular orbital theory (MOT), where PANi (P*) acts as an electron donor whereas the nitramines (NAs) act as electron-deficient species [16]; during co-agglomeration, these electronically charged species form the temporarily excited complex (P + .NM −) [15]. The exception is the β-CL20/PANi composite, because of the presence of a high number of nitro groups in the molecule, bonded at the crowded globular 2,4,6,8,10,12-hexanitro-2,4,6,8,10,12-hexaazaisovurtzitane skeleton, with internal interactions between these nitro groups, makes the β-CL20 molecule not well accessible to the PANi chain mainly for steric reasons.

The higher-moiety electrons at aza-nitrogen atoms in the CL20 nitramino groupings might contribute an inductive effect to decrease the affinity of nitro-nitrogen atoms (see Scheme 2) to π-electrons from PANi (see Scheme 1), which should lower the driving force for the charge transfer. A bigger part of the CL20 molecule should be balanced by internal π–π stacking, its short contacts in crystal lattice should partially remain and thus some amount of the physical mixture of β-CL20 with PANi be formed in the composite [16]. These facts influence all of its thermochemical, detonation, and sensitivity properties (energetic properties are discussed in the next sections). FTIR has also revealed a peak at 675 ± 20 cm^{-1}, attributable to $-HSO_4^-$, a small amount of which is present here; elemental analysis has confirmed the presence of 0.02–4.00% of sulfur and a higher amount

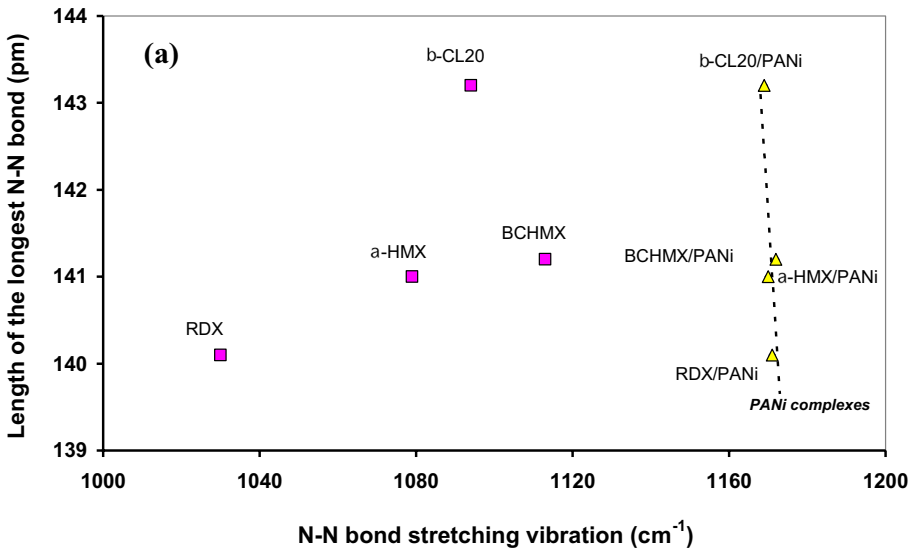

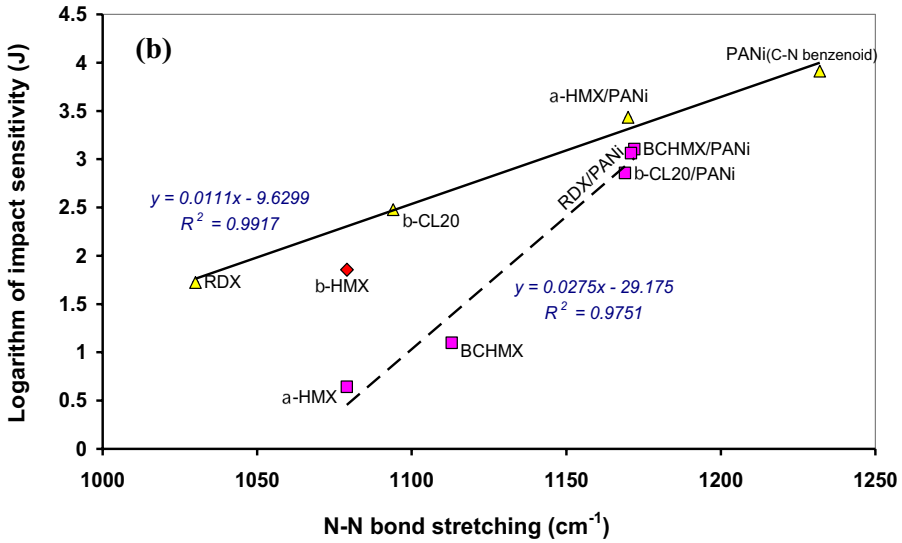

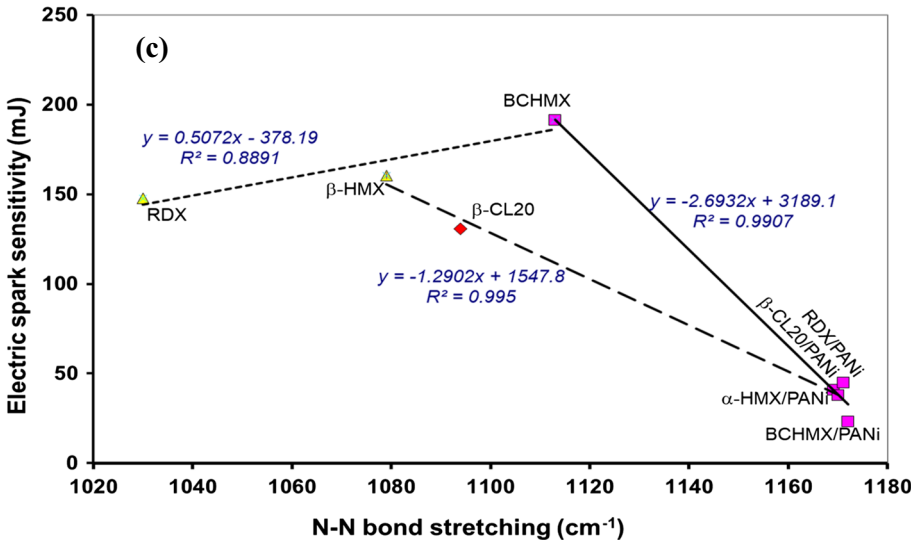

Fig. 5 N–N bond-stretching dependences. **a** A comparison of the lengths of the longest N–N bonds and the stretching vibrations of these bonds of pure nitramines and their composites with PANi (the data placement in this figure indicates the existence of complexes with charge transfer in the sense of Scheme 1); the N–N bond lengths have been taken from the ORTEP views of the nitramines used in the CCDC database shown in section S2.11—Figs. S5(a–e) in the Supplementary Information. **b** Semilogarithmic correlation with impact sensitivity, expressed as drop energy for the 50% probability of initiation (for PANi, C–N bond stretching in benzenoid and quinonoid structures has been used); and **c** the correlation with electric-spark sensitivity, taken here as the energy of spark needed for the 50% probability of initiation

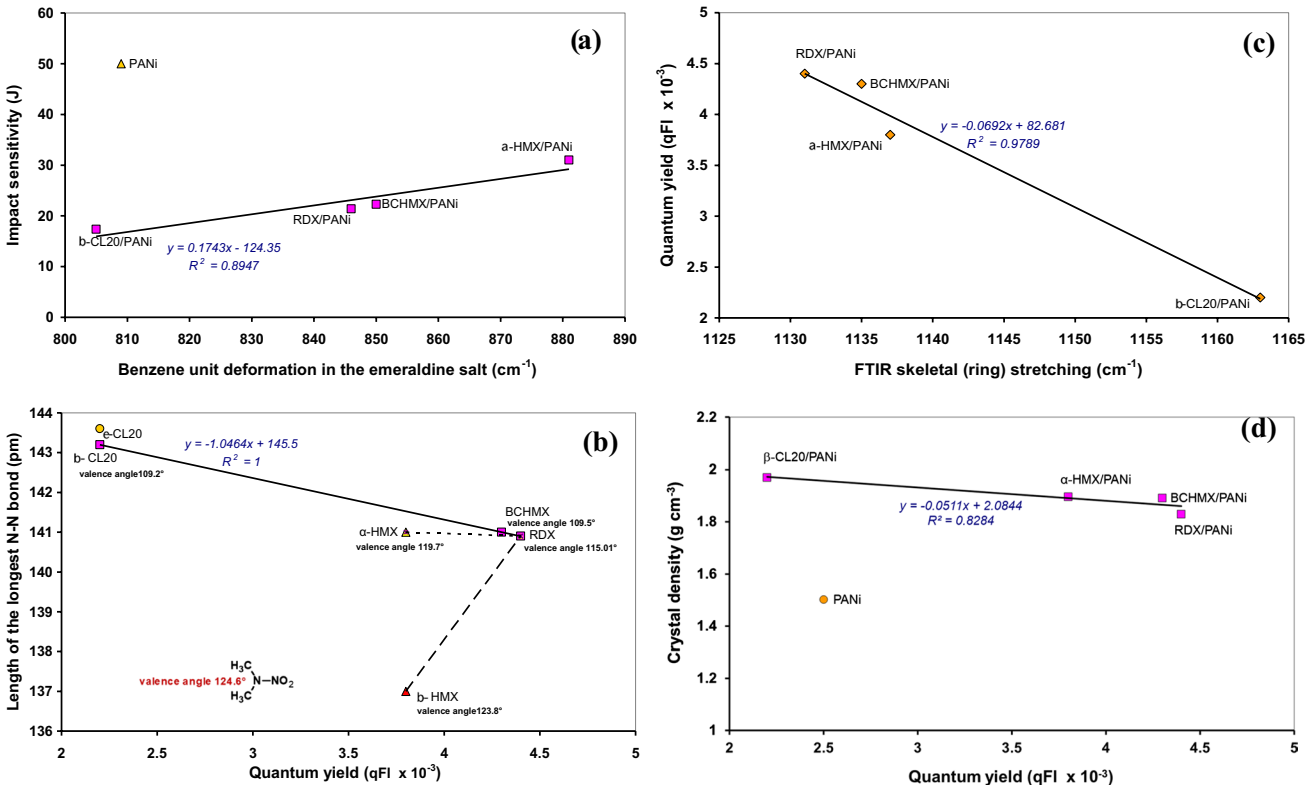

Fig. 6 Dependences connected with structural characteristics: **a** the relationship between impact sensitivity (expressed as drop energy in J) and the benzene-unit deformation in emeraldine salt; **b** the relationship between the length of the longest N–N bond and the relative fluorescence quantum yield (RFQY) from fluorescence measurements (PANi complexes are indicated only by pure-nitramine codes; dimethylnitramine is presented as a standard for valence angles)—for the values of the N−N bond length and valence angles, see the Supplementary Information Fig. S6 (a–g); **c** the relationship between the RFQY from fluorescence measurements and FTIR skeletal (ring) stretching; and **d** the relationship between the crystal density of NAs/PANi complexes and their RFQY

of oxygen. All analyses indicate the presence of sulfur in the form of $-HSO_4^-$, which further balances the complete PANi chain. This anion also helps remove π–π stacking here, which facilitates electron mobility due to this increase in electron density in the polymeric chain. This is further utilized in the interaction with the nitramines forming complexes/composites. It also enhances such physical properties as processability, solubility, and electrical conductivity of PANi as well as its NA composites. Considering polymer-oriented applications like the use for sensor activity based on electrical conductivity and fluorescence, this property is good [15–18]. However, the corresponding composites are more sensitive to electric sparks than pure NAs (see the discussion of sensitivity).

4.4 N−N bond stretching vibrations

The first step in the verification of co-crystal formation in recent papers [19–21] consisted of comparing the lengths of the longest N−N bonds with the stretching vibrations of N−N bonds (Fig. S6 in Supplementary Information). For PANi complexes, this approach is presented in Fig. 5a. In the first approximation here, these bond lengths in pure nitramines were applied to the corresponding PANi composites. It is understandable that due to the formation of the charge-transfer complex of nitramines with PANi, the N−N bond lengths should be changed as a result of the negative influence of the mesomeric equilibrium (Scheme 3) in the nitramine grouping (because of the changes in the force ratios in the crystal lattice of nitramines). Like in the case of co-crystals [19, 20], Fig. 5a shows a large difference between pure nitramines and their NAs/PANi (more precisely their composites). Nevertheless, a comparison of this figure with similar ones in recent papers [19, 20] shows the difference between the PANi composites from CACs of the co-crystal type. Whereas values of the N−N bond stretching of composites lie in the range of 1169–1172 cm^{-1}, in the case of the co-crystals of the nitramines studied it is 940–1040 cm^{-1}. The reason for this is the difference in the decisive intermolecular interactions in the mixed crystals of both groups, which is reflected in the thermochemical, explosive, and sensitivity properties of the composites (as mentioned above).

In the process of nitramine initiation, it is primarily the N−N bond that is homolyzed [42–44]. In this context, the

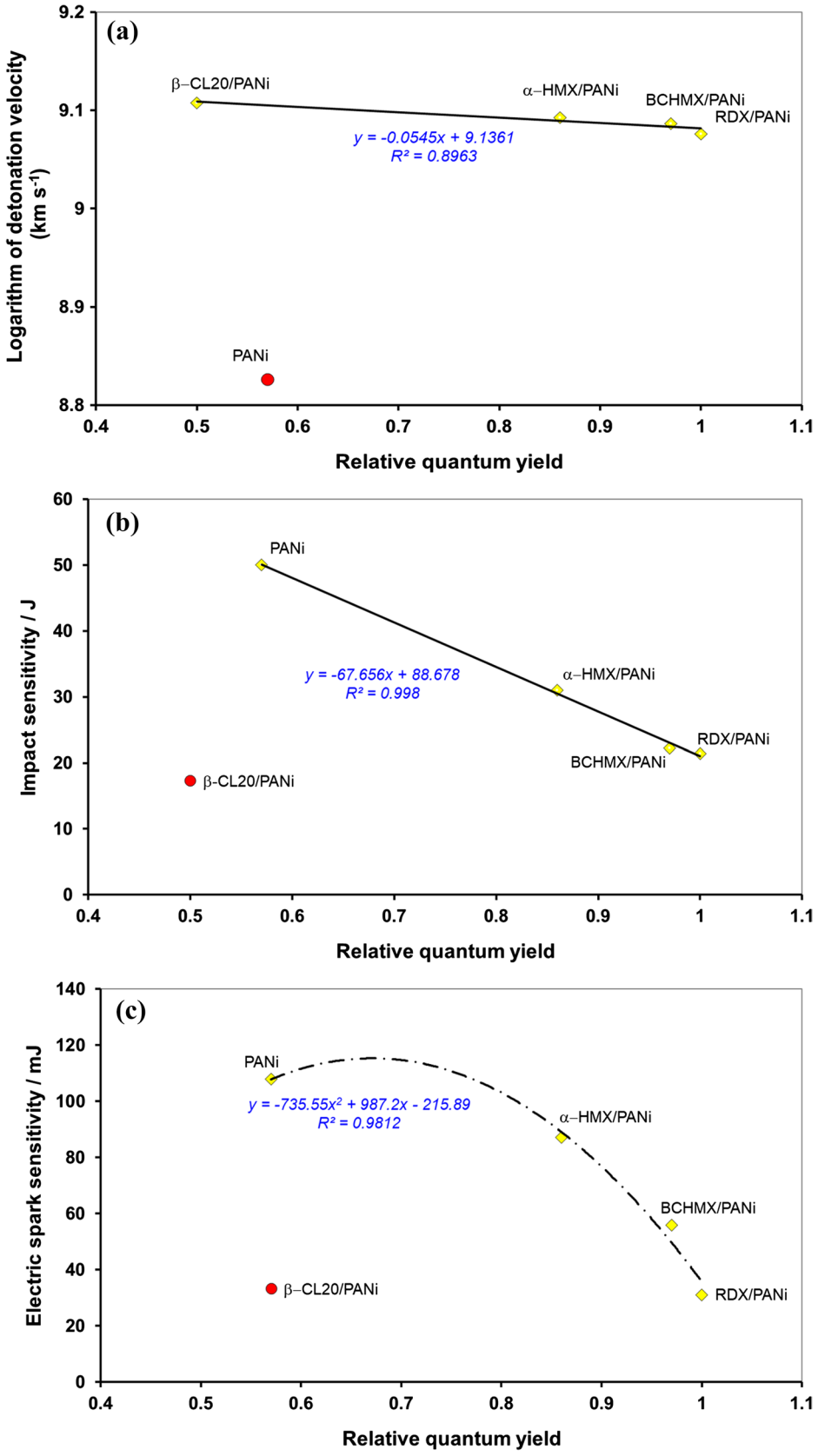

Fig. 7 The dependences connected with the relative fluorescence yield (RFQY / QY) of the NA/PANi complexes studied. **a** The semilogarithmic relationship between detonation velocity and the RFQY; **b** the relationship between impact sensitivity, expressed as drop energy (in J), and QY; and **c** the relationship between electric-spark sensitivity and the QY

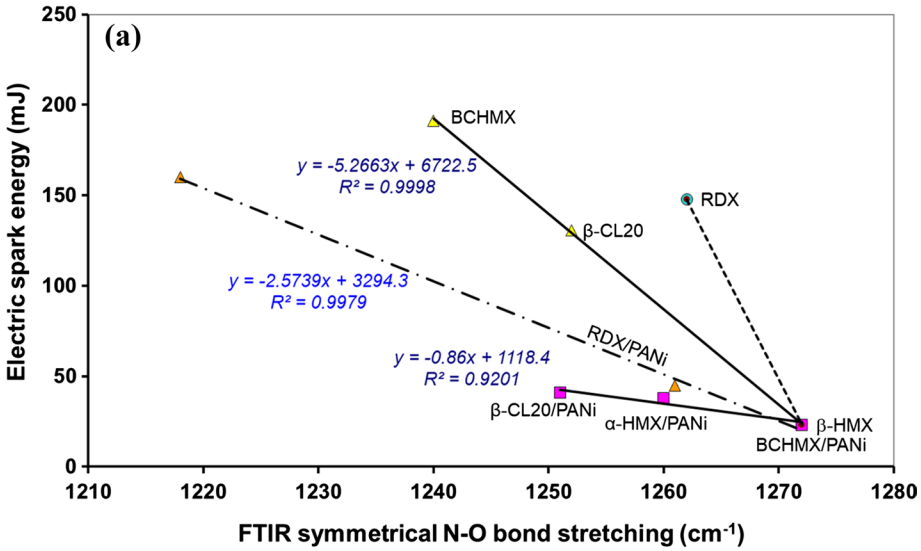

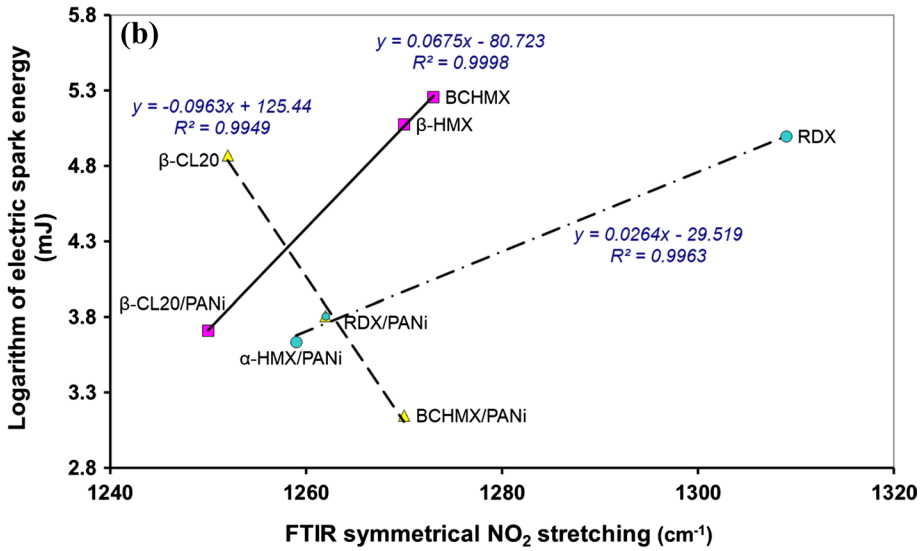

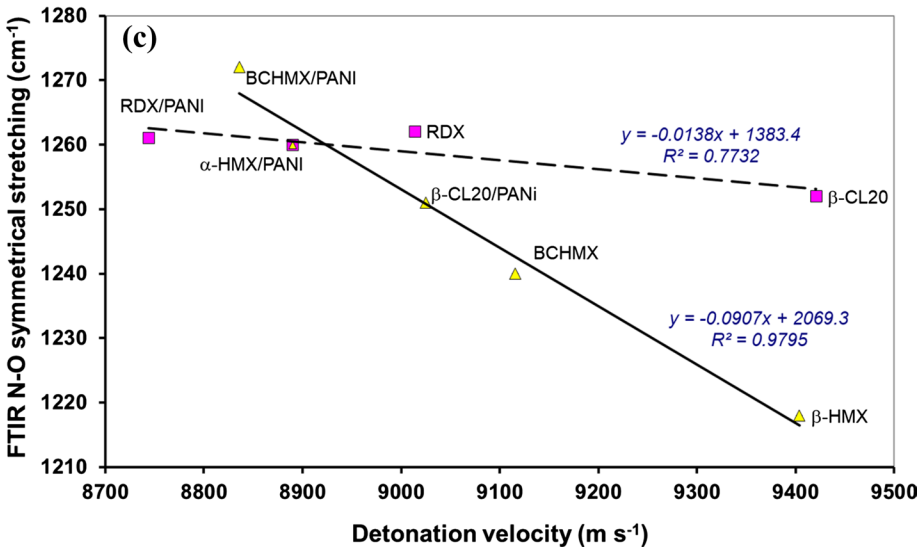

Fig. 8 The dependences connected with the FTIR outputs of the nitro group in the composites studied. **a** The relationship between the energy of the electric spark (needed for the 50% probability of initiation) and FTIR symmetric N–O bond stretching (in the case of RDX, the dashed line indicates its potential affiliation); **b** the semilogarithmic relationship between the energy of the electric spark (needed for the 50% probability of initiation) and FTIR symmetric NO_2 stretching; and **c** the relationship between the FTIR symmetric N–O bond stretching and detonation velocity

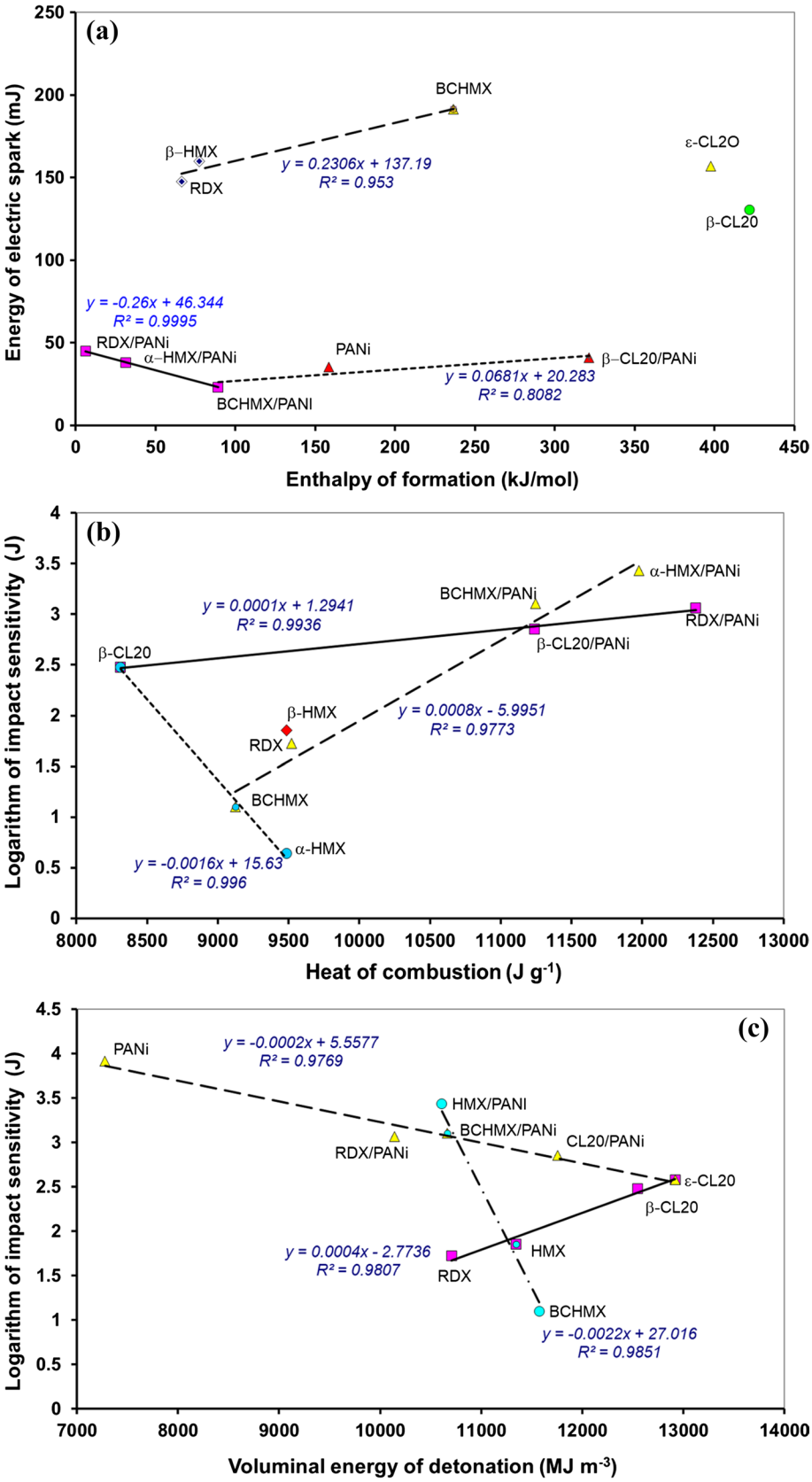

Fig. 9 The dependences connected with the thermochemical aspects of the substances studied. **a** The relationship between the energy of the electric spark (needed for the 50% probability of initiation) and the enthalpy of formation of the nitramines and their composites studied; **b** the semilogarithmic relationship between the impact sensitivity (expressed as drop energy in J) and the heat of combustion of the nitramines and their composites studied; and **c** the semilogarithmic relationship between the impact sensitivity (expressed as drop energy in J) and the voluminal energy of detonation of the nitramines and their composites studied

Table 8 The sensitivity and explosive properties of pure substances and the corresponding CACs

Explosive		Impact sensitivity, E_{dr}			Electric-spark sensitivity	Detonation velocity	Detonation pressure	Energy of detonation	Additive value
No	Code design	E_{dr}, 50% (J)	Ref	E_{dr}, 95% (J)	E_{ES} (mJ)	D (m.s^{-1})	P (GPa)	E_{deton} (J.g^{-1})	E_{deton} (J.g^{-1})
1	RDX	5.6	[38, 41]		147.7	9014	33.91	5915	
2	BCHMX	3.0	[38]		191.4	9116	36.19	6223	
3	α-HMX	1.9	[41]			9126	35.05	5904	
4	ß-HMX	6.4	[38, 41]		160.0	9404	38.00	5964	
5	ε-CL-20	13.2[a]	[39]		157.0	9650	43.41	6303	
		4.1[b]	[40]						
6	ß-CL-20	11.9	[39]		130.6	9421	40.77	6320	
7	PANI	50.0	Cw	108.0	35.6	6813	16.61	4845	
8	57 CL20/PANi	17.4	Cw	33.4	40.9	9025	38.05	5971	6136
9	58 HMX/PANi	31.0	Cw	87.2	37.9	8890	35.30	5597	5876
10	59 BCHMX/PANi	22.3	Cw	55.9	23.2	8836	34.58	5638	5908
11	60 RDX/PANi	21.4	Cw	31.1	44.9	8744	33.26	5544	5805

[a]The value for pure ε-CL-20

[b]The value for the "common" (technical) quality of ε-CL-20

semilogarithmic relationship between impact sensitivity and N−N bond stretching is understandable (Fig. 5b): If it is considered the definitional relationship between vibrational frequency and the bond-force constant (i.e., roughly the strength of the given bond) [45], the relationship in Fig. 5b implies that an increase in this strength should correspond to a decrease in impact sensitivity, which corresponds to the reality. The fact that the β-HMX data do not correlate here while the α-HMX data do also corresponds to the reality (α-HMX is present in the corresponding PANi complex). Similarly, Fig. 5c may be discussed for pure nitramines, although the initiation by an electric spark is related to the addition of an electron to the nitro group [35] and the N−N bond could function here as a conductor of the inductive effect. The formation of the PANi complex, however, is related to a sharp increase in electric-spark sensitivity, perhaps because of the "good transporter" of electrons into the NA reaction center through the conducting PANi chains. The fact that the position of the β-CL20 data indicates the opposite may be related to the complicated structure of its PANi complex (see mentioned above).

4.5 New, unusual dependences

What is interesting are the dependences presented in Fig. 6, which cannot be considered for the CACs of co-crystal nature [6, 19, 20]. Therefore, Fig. 6a shows the proportional influence of the deformation vibrations of the structural building units of the PANi chain on the resistance against the impact of the studied nitramine/PANi complexes. While β-CL20 slightly reduces these deformations when compared to the same ones of the pure PANi, the remaining nitramines show a more pronounced opposite effect. The effect of CL20 is undoubtedly caused by the above-mentioned special structure of its complex with PANi, whereas the RDX, BCHMX, and HMX behavior is a result of the interaction with polyaniline as shown in Scheme 1. The intensity of this interaction can be assessed by fluorescence measurements: As the fluorescence of the NA/PANi complex increases, the intensity of the interactions between the molecules of its co-formers decreases (the opposite is true for the quantum yield) [15–18]; in Fig. 6a, this intensity should thus decrease in the series of RDX-BCHMX-HMX/complexes, with CL20 being an exception, as was mentioned. If the photons are emitted from the nitramine grouping—N−NO_2 of nitramine, the emission is, of course, greatly influenced by its electron configuration, which in the first approximation in Fig. 6b can be represented by the length of the longest N−N bond (the trigger bond) and by the valence angle −CH_2−N−CH_2− connected with this bond. Considering those angles, compared to the valence angle of dimethyl nitramine (taking it as a standard), it is evident that all nitramines (except for β-HMX) have crowded molecules (even RDX, corresponding to its reactivity when compared to β-HMX). The stabilization of the highly sensitive α-HMX by converting it into a PANi complex makes it a very attractive low-impact-sensitive explosive, whose data in Fig. 6c lie logically close to the dependence of the other NA/PANi. The order of the

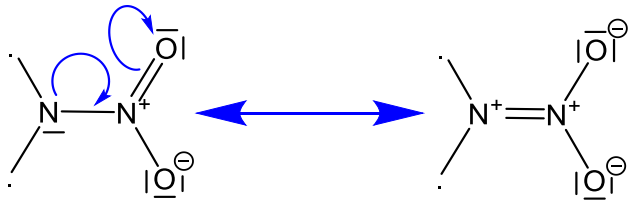

Scheme 3 The mesomeric effect in the nitramine grouping

Ns/PANi complexes in this figure corresponds to the order of the quantum yields found, i.e., the order of the intensity of the intermolecular interactions of the co-formers of the complexes studied (the weakest for β-CL20, the strongest for RDX). The above-mentioned emission order, i.e., the decrease in photon emission with increasing FTIR skeletal stretching (the stretching increases with the increasing steric crowding of nitramine molecules) is also very well-captured in Fig. 6c. The logical linear relationship between the quantum yield and crystal density, presented in Fig. 6d, is also related to the above, i.e., to the electron configuration on nitramine grouping; this configuration is the result of the spatial arrangement and the overall electron structure of the NA molecule, which has a major influence on the method of its placement in the crystal lattice and thus on the density of the crystal.

4.6 The relationships derived from fluorescence measurements

As mentioned in the discussion of Fig. 6, this is the quantum yield, i.e., according to the IUPAC definition [46], the number of certain events per photon absorbed by the system. In the discussion of the above-mentioned figure, it was stated that the electron configuration on the nitramino (trigger) grouping has a fundamental influence on photon emission, which gives the RFQY. Figure 7 shows further interesting relationships between quantum yields and the characteristics of the NA/PANi complexes.

The dependence in Fig. 7a confirms the fact that the detonation characteristics are related to the electronic configuration of the ground state and steric conditions in the reaction center of the molecule [2, 43, 44]. This also concerns the impact sensitivity in Fig. 7b, with the exception of the CL20 complex, which has the weakest mutual interaction of co-formers (and thus different reactivity), as mentioned above. No form of linear relationship could be found for electric-spark sensitivity (Fig. 7c); as noted above, the primary step in this initiation is the addition of an electron to the nitro group [35], i.e., the attack on only a part of the nitramino grouping, which might be the reason for this non-linearity. The difference in the correlation (non-correlation) of the β-CL20/PANi data in each part of Fig. 7 also lies in the strength of the initiation, i.e., the shock in detonation versus the impact and spark in the other two. It appears that these kinds of outputs from fluorescence measurements could be used to study the primary processes of the initiation of energetic materials in the sense of physical organic-chemistry approaches [43, 44].

4.7 Towards the electric-spark and impact sensitivity, including impact influence

As shown in Scheme 2, there are two kinds of crystal arrangements of the PANi composites (verified by spectroscopic and morphological analyses). The stress of the drop hammer should initially be transferred to the PANi layer, by which it can be partially absorbed; once it reaches the NAs, the effect will decrease. In both cases of crystal arrangements, the PANi thus acts as an effective phlegmatizer, well-compatible with HMX, followed by BCHMX, RDX, and CL20. One of the first studies of impact sensitivity in crystalline explosives, using the Raman vibrational spectra, was published by McNesby and Coffey [47]; their approach, through the construction of vibrational energy level diagrams, led to a model designed to calculate the rate of energy transfer from phonon and near-phonon vibrational-energy levels to higher-energy vibrational levels. Unlike them, we tried to correlate this sensitivity directly with the outputs of Raman and FTIR spectroscopy, as presented in [6, 19, 20] and here in Figs. 10b and 6a, newly extended by the output of fluorescence measurements (Fig. 7b). The goal is to search for and confirm trigger bonds. It was pointed out in the discussion of Fig. 5a that because of the difference in the crucial intermolecular interactions in PANi composite crystals and co-crystals with polynitro-co-formers (for the latter, see [6, 19, 20]), the range of the direct relationships of both Raman and FTIR outputs with the initiation characteristics of these composites is somewhat limited.

The mode of interaction of electrically conductive PANi with NA molecules (see Scheme 1) enables perfect electron transport from the electric discharge into the reaction centers of nitramino groupings, i.e., to nitro groups. In addition, the presence of the HSO_4^-anions in PANi enhances its electrical conductivity [15, 18] (see the discussion of the energy aspect). The same group gives PANi stability and processability when it comes to its physical stability and storage, including those of its composites. In the cited papers [9, 10], the mentioned good conductivity of PANi is used to reduce the static-charge accumulation in the mechanistic mixtures of PANi and EMs, i.e., to increase the safety of handling these powder mixtures.

In connection with the attack of the electron on the nitro group, as a primary step of initiation, Figs. 8a and 8b might be of interest. In the first case, according to the proposed mechanism of electron entry in the nitro group [35], the

enhancement of the N–O bond (see the bond-force constant in Section "4.3.1") should facilitate the homolysis of the $N{-}NO_2$ bond, which means that the dependence in Fig. 8a should essentially correspond to the said assumption. On the other hand, Fig. 8a should represent the stabilization of the NO_2 group against the electron addition for partial relations with a positive slope. The introduction of sterically crowded β-CL20 and BCHMX molecules into the PANi composites does not change their stretching much (when compared to the same for HMX and RDX). Therefore in the case of negative-slope dependence, a certain role should also be played by the geometrical details of the respective PANi complexes with charge transfer.

As far as the effect of impact on the initiation of the composites studied is concerned, this could be presented in the first approximation by Fig. 8c. Again, when taking into account the force constant of the bond, it can be stated that the detonation rate of the respective nitramine or its composite increases with a decrease in the N–O bond strength (the opposite to electric-spark initiation according to Fig. 8a) and, as shown in Fig. 7a, with a decrease of electron emission in fluorescence measurement.

4.8 The energy aspects

The detonation parameters of PANi in Table 8 may be somewhat surprising. This polymer is an energetic material with very slow exothermic decomposition (see Table 3 and paper [48]), whose thermochemical characteristics, elemental composition, and density (see Table 7), when inserted into the CHEETAH code, give the values shown. However, this does not mean that PANi is a powerful explosive, but it may

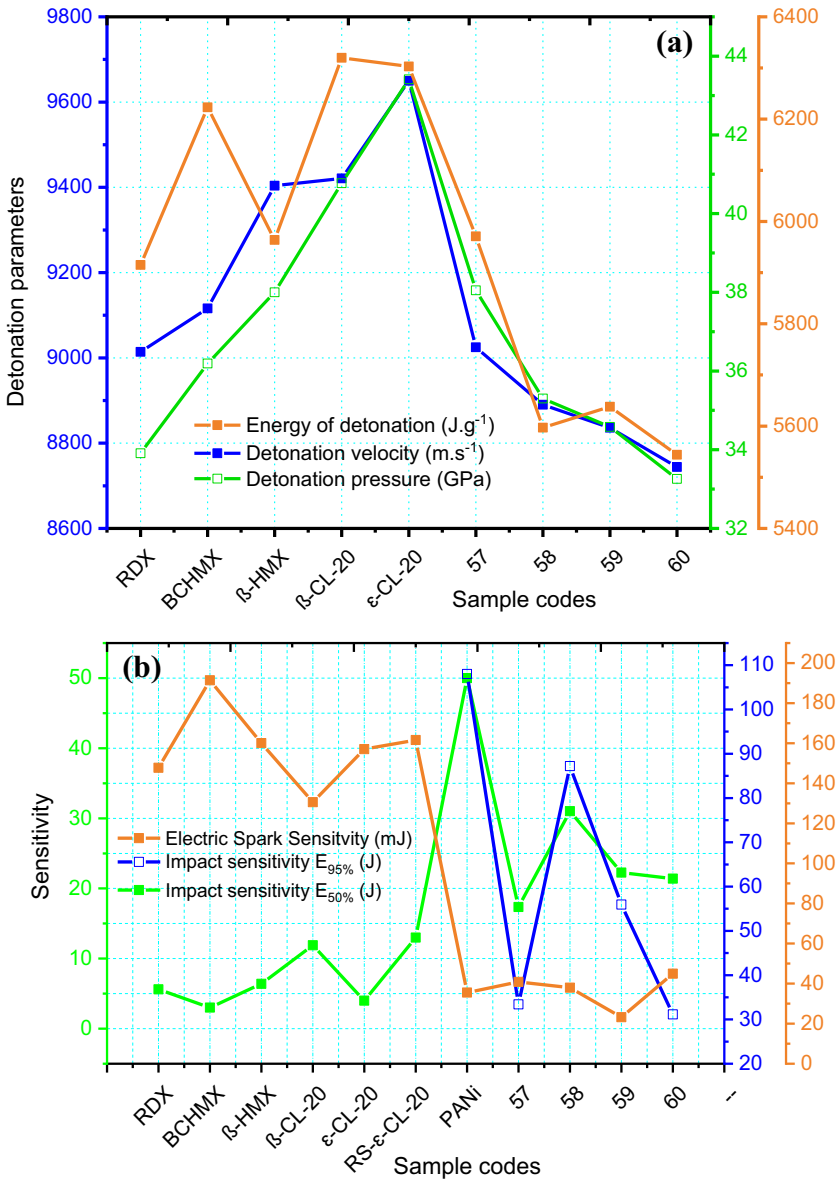

Fig. 10 A comparison of the explosive parameters obtained. **a** The detonation parameters of the CACs with the pure nitramines used for the preparation. **b** A comparative graphical representation of impact and electric-spark sensitivity

be detonated in a larger charge diameter and with a very powerful initiation.

It is a well-known fact that the mixing of two explosives results in a mixture that usually has a higher detonation rate than would correspond to the percentage of components in this mixture (it is also valid for some inert admixtures) [49]. Prof. Urbanski [49] explains these increases in values by the increase in the entropy of the resulting mixture caused by the components entering it. For this kind of evaluation, it used the energies of detonation, E_{deton} (see Table 8, where the additive value of E_{deton}) [6, 19, 20]. When compared to nitraminic co-crystals with polynitroaromatic co-formers [19, 20], the effect of the increase in these "percentage" (additive) E_{deton} values, due to the PANi-composite formation, is more pronounced (for the case of only nitramine co-formers, this effect is opposite [6]).

The inverse relationship between the performance [1, 2] and/or the energy content [3, 4, 50] of explosives and their sensitivity has been mentioned (Licht's rule [1]). What this situation is like in the case of the composites studied here is shown in Fig. 9.

It should be prefaced that pure cyclic nitramines (except for BCHMX) are an exception to Licht's rule [2], as can be seen in all the illustrations of Fig. 9a–c. This exception still awaits scientific explanation. The sensitivity to electric spark versus to the enthalpy of formation (Fig. 9a) [3, 4] is consistent with expectations, with the exception of β-CL20/PANi, whose specific structure has been mentioned above and which might be a reason for this expectation. It is quite possible that during the initiation of the composites, the PANi itself is simultaneously attacked by the discharge. It might be worth mentioning here that in nitramines, the energy of an electric spark is semi-logarithmically proportional to the length of the longest N−N bond in their molecules [35] (which may also determine the position of the β-CL20/PANi data in Fig. 9a).

The relationship between impact sensitivity and energy content is presented in a semilogarithmic version in Fig. 9b, where the energy content, represented by the heat of combustion [50], increases from the right to the left and, except for the pure nitramines β-CL20, BCHMX and α-HMX, is in full agreement with Licht's rule. The same concerns Fig. 9c [2].

A synoptic overview of the results of the study of the sensitivity and the explosive characteristics of the composites and nitramine compositions is provided in Fig. 10.

5 Conclusions

Composite microparticles of electrically conductive polyaniline (PANi) with the attractive cyclic nitramines RDX, HMX, BCHMX, and CL20 were prepared by co-precipitation followed by co-agglomeration of the resulting co-precipitates. They are essentially charge-transfer complexes, which is the reason for their slightly lower thermal stability in comparison with the starting nitramines. Spectral and differential thermal analysis techniques have shown changes in polymorph modifications in CL20 (from ε to β) and HMX (from β to α) during this preparation. These microcrystals have smoothed surfaces and two major kinds of crystals, namely center-core and superficially coated, the latter of which has made the nitramine crystal edges rounded. The coating of microcrystals significantly reduces their impact sensitivity, especially in the case of HMX (with drop energy increasing from 6.4 J in ß-HMX to 31 J in α-HMX/PANi versus the extreme impact sensitivity of 1.9 J for α-HMX in its pure state). The FTIR symmetric NO_2 and N−O bond stretching, the N−N bond stretching, and newly the quantum yield from fluorescence application in the composite microcrystals are logically associated with their initiation reactivity (i.e., impact and electric-spark sensitivity), related to the nitraminic components of composites. The relationship between impact sensitivity and the benzene-unit deformation in the emeraldine salt of PANi chains as well as linear logical relationships between detonation rates and both the FTIR symmetric N−O bond stretching, and the relative fluorescence quantum yield, have also been found and explained. In comparison to pure nitramines, the PANi electrical conductivity has significantly increased the electric-spark sensitivity of composites. Pure polyaniline and its composites are also highly sensitive to laser power above 29 mV with a grating of × 10/0.25. The relationships between the sensitivity parameters and the energy content or power of PANi composites are essentially consistent with Licht's rule. The prepared composites are characterized by an unusually high crystal density and good detonation parameters; the increase in the detonation parameters of explosive mixtures after mixing their components is more pronounced in PANi composites than in common energetic co-crystals. The interesting sensitivity characteristics of PANi composites, together with their easy preparation, should predetermine their potential use as components of various types of lead-free initiators for different types of charges, especially in "green" electric detonators and squibs.

Supplementary Information The online version contains supplementary material available at https://doi.org/10.1007/s42114-024-00936-0.

Author contribution Veerabhadragouda B. Patil and Svatopluk Zeman wrote the main part of the manuscript. Veerabhadragouda B. Patil made the experimental design and did the experiment on the preparation and characterization part. Oldřich Machalický did the fluorescence measurements. Petr Bělina did the PXRD and particle size analysis part. Roman Svoboda did the Raman measurements. Waldemar A. Trzcinski calculated detonation parameters. Veerabhadragouda B. Patil and Svatopluk Zeman realized the discussion, conclusion, and active participation in the manuscript revision. All authors reviewed the manuscript and agreed.

Funding Open access publishing supported by the National Technical Library in Prague. Funding was provided by the Univerzita Pardubice, Student Grant Project no. SGS_2022_003.

Data availability The raw data/findings will be available upon reasonable request to the corresponding author.

Declarations

Conflict of interest The authors declare no competing interests.

References

1. Licht H-H (2000) Performance and sensitivity of explosives. Propellants Explos Pyrotech 25:126–132. https://doi.org/10.1002/1521-4087(200006)25:3%3c126::AID-PREP126%3e3.0.CO;2-8
2. Zeman S, Jungova M (2016) Sensitivity and performance of energetic materials. Propellants Explos Pyrotech 41(3):426–451. https://doi.org/10.1002/prep.201500351
3. Zeman S (2019) Influence of the energy content and its outputs on sensitivity of polynitroarenes. J Energ Mater 37(4):445–458. https://doi.org/10.1080/07370652.2019.1634159
4. Zeman S (2022) The influence of energy content and its outputs on the impact sensitivity of high-nitrogen energetic materials. J Energ Mater 40(1):1–14. https://doi.org/10.1080/07370652.2020.1822463
5. Elbeih A, Zeman S, Jungova M, Vavra P (2013) Attractive nitramines and related PBXs. Propellants Explos Pyrotech 38(3):379–385. https://doi.org/10.1002/prep.201200011
6. Patil VB, Yan QL, Trzcinski WA, Bělina P, Shánělová J, Musil T, Zeman S (2022) Co-agglomerated crystals of cyclic nitramines with sterically crowded molecules. CrystEngComm 24:7771–7785. https://doi.org/10.1039/D2CE00840H
7. Ang HG, Pisharath S (2012) Energetic polymers: binders and plasticizers for enhancing performance. Willey-VCH Wenheim
8. Shimano JY, McDiarmid AG (2001) Polyaniline, a dynamic block copolymer: key to attaining its intristic conductivity? Synth Met 123:251–262. https://doi.org/10.1016/S0379-6779(01)00293-4
9. Fathollahi M, Lotfzadeh H, Khorasanloo FH, Hosseini SG (2022) Investigation of the effect of polyaniline additive on reducing static charge accumulation in HMX and PETN explosives. J Appl Chem (Tehran) 17(62):139–154. https://doi.org/10.22075/CHEM.2022.21402.1897.(in Persian)
10. Gibot P, Bach A, Vidal L, Schnell F, Gadiou R, Spitzer D (2017) Safer and performing energetic materials based on polyaniline-doped nanocomposites. J Energ Mater 35(2):136–147. https://doi.org/10.1080/07370652.2016.1210697
11. Namsheer K, Rout CS (2021) Conducting polymers: a comprehensive review on recent advances in synthesis, properties and applications. RSC Adv 11:5659–5697. https://doi.org/10.1039/D0RA07800J
12. He G, Yang Z, Zhou X, Zhang J, Pan L, Liu S (2016) Three-dimensional graphite filled poly(vinylidene fluoride) composites with enhanced strength and thermal conductivity. Comp Sci & Tech 131:22–31. https://doi.org/10.4028/www.scientific.net/kem.842.63
13. Yu L, Ren H, Guo X, Jiang X, Jiao Q (2014) A novel ε-HNIW-based insensitive high explosive incorporated with reduced graphene oxide. J Therm Anal Calorim 117:1187–1199. https://doi.org/10.1007/s10973-014-3928-7
14. Niu C, Jin B, Peng R, Shanga Y, Liu Q (2017) Preparation and characterization of insensitive HMX/rGO/G composites via in situ reduction of graphene oxide. RSC Adv 7(51):32275–32281. https://doi.org/10.1039/C7RA03863A
15. Patil VB, Nadagouda M, Tur S, Yelamaggad C, Abbaraju V (2021) Detection of energetic materials via polyaniline and its different modified forms. Polym Adv Technol 32(12):4663–4677. https://doi.org/10.1002/pat.5458
16. Patil VB, Ture S, Yelamaggad C, Nadagouda CM, Venkataraman A (2021) Turn-off fluorescent sensing of energetic materials using protonic acid doped polyaniline: a spectrochemical mechanistic approach. Z Anorg Allg Chem 647(4):331–340. https://doi.org/10.1002/zaac.202000321
17. Ture SA, Pattathil SD, Patil VB, Yelamaggad CV, Martinez-Manez R, Abbaraju V (2022) Synthesis and fluorescence sensing of energetic materials using benzenesulfonic acid-doped polyaniline. J Mater Sci-Mater Electron 33:8551–8565. https://doi.org/10.1007/s10854-021-06537-7
18. Ture S, Patil VB, Yelamaggad C, Martinez-Manez R, Abbaraju V (2021) Understanding of mechanistic perspective in sensing of energetic nitro compounds through spectroscopic and electrochemical studies. J Appl Polym Sci 138(32):50776 (http://hdl.handle.net/10251/193937)
19. Patil VB, Zalewski K, Schuster J, Bělina P, Trzcinski WA, Zeman S (2021) A new insight into the energetic co-agglomerate structures of attractive nitramines. Chem Eng J 420:130472. https://doi.org/10.1016/j.cej.2021.130472
20. Patil VB, Bělina P, Trzcinski WA, Zeman S (2023) Co-agglomerated crystals of 2,2′,4,4′,6,6′-hexanitro -stilbene/-azobenzene with attractive nitramines. Chem Eng J 457:141200. https://doi.org/10.1016/j.cej.2022.141200
21. Patil VB, Bělina P, Trzcinski WA, Zeman S (2024) Co-agglomerated crystals of cyclic nitramines with the nitrogen rich 3,6-bis(1H–1,2,3,4-tetrazol-5-ylamino)-1,2,4,5-tetrazine (BTATz). Chem Eng J 483:149029. https://doi.org/10.1016/j.cej.2024.149029
22. Xue ZH, Huang B, Li H, Yan QL (2020) Nitramine-based energetic cocrystals with improved stability and controlled reactivity. Cryst Growth Des 20:8124–8147. https://doi.org/10.1021/acs.cgd.0c01122
23. Klasovitý D, Zeman S (2010) Process for preparing cis-1,3,4,6-tetranitrooctahydroimidazo-[4,5-d]imidazole (bicyclo-HMX, BCHMX). Czech Pat 302068, C07D 487/04, University of Pardubice (in Czech)
24. Liu G, Li H, Gou R, Zhang C (2018) Crystal packing of impact-sensitive high-energy explosives. Cryst Growth Des 18:7065–7078. https://doi.org/10.1021/cg501267f
25. Pouretedal HR, Damiri S, Zandi A (2019) Study the operating conditions on agglomeration of RDX particles in anti-solvent crystallization by using statistical optimization. Def Technol 15(2):233–240. https://doi.org/10.1016/j.dt.2018.09.007
26. Sapurina IYu, M. A. Shishov MA (2012) Oxidative polymerization of aniline: molecular synthesis of polyaniline and the formation of supramolecular structures. In: Gomes ADS (ed),

New polymers for special applications, Ed In Tech. https://doi.org/10.5772/48758
27. Colomban Ph, Folch S, Gruger A (1999) Vibrational study of short-range order and structure of polyaniline bases and salts. Macromolecules 32(9):3080–3092. https://doi.org/10.1021/ma9810181
28. Lakowicz JR (2006) Solvent and environmental effects. In: Lakowicz JR (ed) Principles of fluorescence spectroscopy. Springer, Boston, MA. https://doi.org/10.1007/978-0-387-46312-4_6
29. Stejskal J, Gilbert RG (2002) Polyaniline Preparation of a conducting polymer (IUPAC technical report) IUPAC. Pure Appl Chem 74(5):857–867
30. Fried LE (1996) CHEETAH, 1.39 users' manual UCRL-MA-117541, CA Lawrence Livermore National, Laboratory. (1996)
31. Ficket W, Davies WC (1979) Detonation. In: Zukas JA, Walters PW (eds) Explosives effects and detonation. University of California Press, Berkeley, pp 115–135
32. Hobbs ML, Baer MR (1993) Calibrating the BKW-EOS with a large products species base and measured C-J properties. In: Proceedings of the 10th symposium (international) on detonation, held in Boston, Massachusetts, pp. 409–418.
33. Davis WC, Fickett W (1969) Detonation theory and experiment. Dovrer Publ Inc, New York pp 2–12. https://www.osti.gov/biblio/4785669.
34. Sućeska M (1995) Testing methods of explosives. Springer, Heidelberg, p 176
35. Zeman S, Liu N (2020) A new look on the electric spark sensitivity of nitramines. Def Technol 16:10–17. https://doi.org/10.1016/j.dt.2019.06.023
36. Elbeih A, Pachman J, Zeman S, Vávra P, Trzciński WA, Akštein Z (2012) Detonation characteristics of plastic explosives based on attractive nitramines with polyisobutylene and poly (methyl methacrylate) binders. J Energ Mater 30(4):358–371. https://doi.org/10.1080/07370652.2011.585216
37. Bathlet H, Volk F, Weindel M (2004) ICT Database of thermochemical values, Version 7.0. Fraunhofer Institut für ChemischeTechnologie, Pfinztal, Germany.
38. Storm CB, Stine JR, Kramer JF (1990) Sensitivity relationships in energetic materials. In: Bulusu SN (ed) Chemistry and physics of energetic materials. Kluwer Acad Publs, Dordrecht, pp 605–639
39. Ou Y, Wang C, Pan Z, Chen B (1999) Sensitivity of hexanitrohexaaza¬isowurtzitane. Chinese J Energ Mater (HanNeng CaiLiao) 7:100–108 ((**in Chinese**))
40. Viswanath DS, Ghosh TK, Boddu VM (2018) Hexanitrohexaazaisowurtzitane (HNIW, CL-20). In: Viswanath DS, Ghosh TK, Boddu VM (eds) Emerging energetic materials: synthesis, physicochemical, and detonation properties. Springer, Dordrecht, pp 59–100
41. Atalar T, Jungová M, Zeman S (2009) A new view of relationships of the N-N bond dissociation energies of cyclic nitramines. Part II. Relationships with impact sensitivity. J Energ Mater 27:200–216. https://doi.org/10.1080/07370650802640366
42. Manelis GM, Nazin GM, Rubtsov YuI, Strunin V (1996) Termicheskoe razlozhenie i goreniye vzryvchatykh veschestv i porokhov (Thermal decomposition and combustion of explosives and powders), Izdat. Nauka, Moscow; English edition (2003) Thermal decomposition and combustion of explosives and propellants. Taylor & Francis, London
43. Zeman S (2018) Characteristics of thermal decomposition of energetic materials in a study of their initiation reactivity. In: Vyazovkin S, Koga N, Schick C (eds), Handbook of thermal analysis and calorimetry recent advances, techniques and applications, vol. 6, 2nd edition, Elsevier, Amsterdam, pp 573–612. https://doi.org/10.1016/B978-0-444-64062-8.00006-1
44. Zeman S (2023) The chemical micromechanism of energetic materials initiation. In: Pang W, DeLuca LT (eds) Nano and micro-scale energetic materials, vol. 2, chapter 19, Wiley-VCH, Weinheim, pp 569–624.
45. Kaya S, Kaya C, Obot IB, Islam N (2016) A novel method for the calculation of bond stretching force constants of diatomic molecules. Spectrochim Acta A: Mol Biomol Spectroscopy 154:103–107. https://doi.org/10.1016/j.saa.2015.10.030
46. Compendium of chemical terminology (2021), 2nd ed. (the "gold book"), version 2.3.3, compiled by McNaught AD, Wilkinson A, IUPAC.
47. McNesby KL, Coffey CS (1997) Spectroscopic determination of impact sensitivities of explosives. J Phys Chem B 101:3097–3104. https://doi.org/10.1021/jp961771l
48. Patil VB, Svoboda R, Bělina P, Zeman S (2023) Towards the thermal reactivity and behavior of co-agglomerated crystals of DATB and TATB with attractive nitramines. Thermochim Acta 724:179494. https://doi.org/10.1016/j.tca.2023.179494
49. Urbanski T (1980) On entropy and free energy of explosives (preliminary communication). Bull l'Academie Pol Des Sci, Ser Des Sci Chim 28:511–513
50. Zeman S, Hussein AK, Jungová M, Elbeih A (2018) Effect of energy content of the nitraminic plastic bonded explosives on their performance and sensitivity characteristic. Def Technol 15:488–494. https://doi.org/10.1016/j.dt.2018.12.003